TERRESTRIAL HEAT FLOW AND CRUSTAL RADIOACTIVITY IN NORTHEASTERN NEW MEXICO AND SOUTHEASTERN COLORADO

by

C. L. Edwards

Submitted in Partial Fulfillment
of the Requirements for the Degree of
Doctor of Philosophy
in Geoscience

NEW MEXICO INSTITUTE OF MINING AND TECHNOLOGY

Socorro, New Mexico

August, 1975

TABLE OF CONTENTS

LIST OF TABLES

LIST OF FIGURES

ACKNOWLEDGEMENTS

I wish to thank Dr. Marshall Reiter, Chairman of the Advisory Committee, for his suggestions and constructive criticism of the research and original manuscript. I wish also to thank the other members of the Advisory Committee, Dr. Allan Sanford, Dr. Alan Sharples, Dr. Kent Condie and Dr. Charles Chapin, who offered advice and guidance throughout the research. Appreciation is due Dr. Allan Gutjahr for his assistance with the experimental problems associated with the gamma ray spectrometer. Thanks are also due to my wife for her help and encouragement throughout the research.

This work was supported by National Science Foundation Grant GI-32482, New Mexico Energy Research and Development Program Proposal #5, and New Mexico Institute of Mining and Technology - the Geoscience Dept. and the New Mexico Bureau of Mines and Mineral Resources. Some of the equipment used was purchased on Bureau of Reclamation Contract #14-06-500-1875. Salary for a student to operate the gamma ray spectrometer was supported by New Mexico Water Resources Institute Grant 3109-405 funded by New Mexico Energy Research and Development Program.

The following organizations gave permission to log boreholes on their property and/or under their supervision. The help and cooperation of individuals associated with these companies is gratefully acknowledged: American Fuels, AMOCO, CONOCO Minerals, Ben Donegan, Duval, Inspiration Development, Kaiser Steel, Eileen McGrath, Molycorp, National Park Service, USGS, Wesley Young.

ABSTRACT

New heat flow data obtained in northeastern New Mexico and southeastern Colorado show: 1) In northern New Mexico and southern Colorado a broad heat flow anomaly associated with the Southern Rocky Mountain complex contrasts with a sharp narrow heat flow anomaly between Santa Fe and Socorro, New Mexico, apparently associated only with the Rio Grande rift; 2) The relatively high heat flow region apparently associated with the Southern Rocky Mountains, extends 200-300 km onto the Great Plains of northeastern New Mexico and southeastern Colorado; 3) There is a complex relationship between heat flow and extensive volcanic activity, that is, areas of extensive volcanic activity do not necessarily have high heat flow. Measurements of crustal radioactivity in the vicinity of the Rio Grande rift suggest that the radioactive heat generation contributes uniformly to the surface heat flow. This implies that the heat flow patterns observed along the Rio Grande rift are caused by tectonic and volcanic sources and not by variations in crustal radioactivity.

INTRODUCTION

The temperature distribution and the distribution of radioactive heat producing elements in the crust and upper mantle are important parameters to be considered while analyzing geological processes (Birch, 1947). Jeffreys (1952) indicates that all models of the earth's thermal history must satisfy the boundary condition of the average heat outflow of the earth at the present time. Measurements of terrestrial heat flow coupled with measurements of heat production due to radioactive decay in the crust form important boundary conditions that must be met by models derived from other geological and geophysical data. For example, the Basin and Range of southwestern New Mexico and southeastern Arizona has low P_n velocities (7.8-8.0 km/sec) possibly indicating a partial melting zone (Herrin and Taggart, 1962; James and Steinhart, 1967). Using measurements of transient geomagnetic variations, Schmucker (1964) suggests a zone of anomalously high electrical conductivity under this area caused by an upwarping of isotherms. Measurement of high heat flow in the area complement the seismic and geomagnetic data (Warren and others, 1969; Decker and Smithson, 1975; Reiter and others, 1975)

To appreciate the interrelationship between the thermal processes in the crust and upper mantle, and the tectonic and volcanic activity within an area, it is necessary to

obtain a high density of heat flow measurements. Whereas measurements on the order of 50-100 km apart may be sufficient to define regional heat flow patterns in a generalized sense, transitions between heat flow provinces and the complex geothermal character within a heat flow province will probably have to be defined with heat flow measurements of the order of 10 km apart. Heat flow transitions occurring in less than 100 km have been reported between the Sierra Nevada and Basin and Range (Sass and others, 1971a; Roy and others, 1968) and between the Basin and Range and the Great Plains (Roy and others, 1972; Warren and others, 1969). Roy and others (1972) indicated that all heat flow transitions studied were sharp, the total change occurring within 100 km. Sass and others (1971a) have identified heat flow subprovinces within the Basin and Range. Reiter and others (1975) suggested a complex geothermal structure in the eastern Colorado Plateau. These subprovinces are suggested to be the result of variations in the crust and upper mantle, for example, the regional high heat flow near the Zuni uplift and the low to normal heat flow region in the San Juan Basin (Reiter and others, 1975).

The purpose of this study was two fold: 1) To map the near surface heat flow in northeastern New Mexico and southeastern Colorado, 2) To measure crustal radioactivity at drillsites in the vicinity of the Rio Grande rift in order to estimate the contribution of crustal radioactive

heating to the total surface heat flow. 65 temperature logs were made in northeastern New Mexico and southeastern Colorado yielding 50 new unreduced heat flow sites (figure 1). 9 new reduced heat flows have been made in the Rio Grande rift and vicinity of New Mexico and southern Colorado.

Figure 1. Heat flow sites in the Four Corners area. Solid diamonds indicate data from Birch (1947, 1950), Lovering (1948), Herrin and Clark (1956), Spicer (1964), Warren and others (1969), Decker (1969), Sass and others (1971a), Costain and Wright (1973). Open diamonds indicate data from M. Chessman and others (in prep.), and M. Reiter and others (in prep.). Solid circles indicate data from Reiter and others (1975). Open circles in Arizona and southwestern New Mexico indicate data from M. Reiter and others (in prep.). Open cirlces in northeastern New Mexico and southeastern Colorado indicate data from this manuscript.

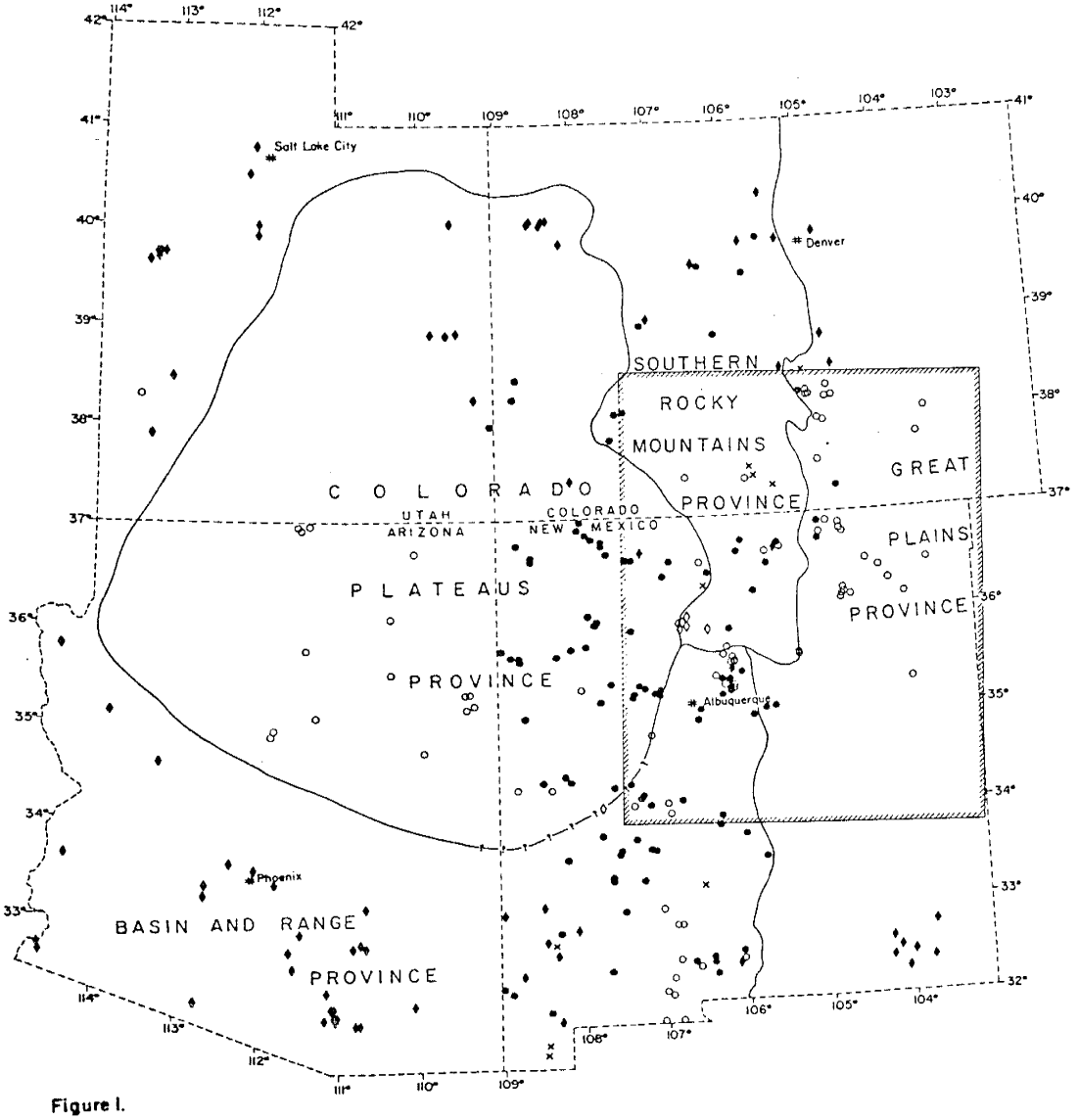

Figure 1.

GEOLOGIC AND GEOPHYSICAL SETTING

Within the area of investigation two different geologic provinces, the Great Plains and the Southern Rocky Mountains are in juxtaposition with the Rio Grande rift. The Wet and the Sangre de Christo Ranges are east of the Rio Grande depression and the San Juan Mountains are west of the Rio Grande rift (Eardly, 1962; Kelley, 1972). The Sangre de Christo uplift extends from central Colorado into New Mexico where it terminates near Santa Fe (Kelley, 1972). The San Juan Mountains rank as one of the most spectacular and complex volcanic fields in the United States. More than 4000 cubic kilometers of calc-alkaline material have erupted in the western San Juan Mountains (Luedke and Burbank, 1968). The Rio Grande rift bisects the Southern Rocky Mountains and consists of a series of north-trending grabens arranged north-northeasterly along the course of the Rio Grande (Kelley, 1952).

The Great Plains, relatively stable since the Mesozoic, contrast with the tectonically active Southern Rocky Mountains, these two provinces meeting in north-eastern New Mexico and southeastern Colorado (Eardley, 1962). The Las Vegas and Raton Basins lie at the western margin of the Great Plains in northeastern New Mexico and southeastern Colorado. Within these basins, sills, dikes, plugs, stocks, sole injections, and laccoliths were intruded into the sedimentary rocks during the Oligocene epoch (Johnson

and others, 1966; Stormer, 1972). Many of these intrusives form mountains, hills, or buttes. Basaltic lava sheets cap the high mesas east of Trinidad, Colorado, and east of Raton, New Mexico (Johnson, 1968). The Spanish Peaks and other large igneous masses dominate the topography of the Raton Basin area but dike systems are more characteristic topographic features (Johnson, 1968). The Sierra Grande Arch, a Precambrian basement high that trends southwest from the northeast corner of the state, is a major tectonic feature in northeastern New Mexico (Sidwell and Warn, 1953).

Extensive basaltic volcanism occurred in the Southern Rocky Mountain vicinity during much of late Cenozoic time (Christiansen and Lipman, 1972). Basalts and basaltic andesites, commonly showing some crustal contamination, were erupted to the east of the Rio Grande rift, (near Raton, Clayton, Capulin, and the Cimarron Mountains), and to the west of the rift, (near Mount Taylor, the Jemez Mountains, the Tusas Mountains and the eastern San Juan Mountains). However, primarily theoleiitic, uncontaminated basalts were erupted within the Rio Grande rift (Lipman, 1969; Lipman and others, 1973).

Sanford (1965) and Sanford and Cash (1969) reported that during the period of January 1, 1962, through December 31, 1967, the strongest shocks in New Mexico occurred in the northeast. Toppozada and Sanford (1972) reported that during the period of January 1968 through June 1971, seismic activity shifted from northeastern New Mexico to

the Rio Grande Valley, a distribution of seismic activity which is in better agreement with the historical records of felt shocks. Sanford and Holmes (1962) showed that the majority of earthquakes in New Mexico occur along the Rio Grande rift. The extreme northwestern, southwestern and southeastern corners of New Mexico are essentially aseismic (Toppozada and Sanford, 1972). Seismic crustal studies (Stuart and others, 1964; Jackson and others, 1963; Stewart and Pakiser, 1962) have shown the crust in the Great Plains of southeastern Colorado and eastern New Mexico to be about 50 km thick. Pakiser (1963) inferred a crustal thickening of about 60 km under the Southern Rocky Mountains. Phinney (1964) postulated that the Moho is at a depth of 35-40 km at Albuquerque, New Mexico, with an intermediate discontinuity at 18-26 km. Sanford and others (1973) reported that a sharp discontinuity, possibly underlain by material of very low rigidity, had been detected at a depth of 18 km near Socorro, New Mexico. The Pn velocities are generally greater than 8.1 km/sec in the Great Plains and about 8.0 km/sec in the Rocky Mountain region (Archambeau and others, 1969).

Schmucker (1964) reported a sharp discontinuity in the character of recorded geomagnetic data along an east-west profile at 32° North latitude, between Las Cruces and Cornudas, New Mexico. Caner and others (1967) discussed deep magnetic data along four east-west profiles at latitudes 32° North, 35° North, 49.5° North, and 51° North.

They suggest that a sharp electrical conductivity discontinuity in the mantle occurs generally near the physiographic boundary between the Rocky Mountains and the Great Plains. However, along the profile through northeastern New Mexico the conductivity discontinuity occurred east of the Great Plains-Southern Rocky Mountain physiographic boundary at Sayer, Oklahoma near the Texas-Oklahoma border. Schmucker (1970) suggested an increase of about 100°C between 50 to 300 km underneath the Southern Rocky Mountains, and perhaps a local upwelling of hot material underneath the Rio Grande rift as the source of the geomagnetic anomaly.

Herrin and Clark (1956) presented six heat flow measurements in the Great Plains of west Texas and southeastern New Mexico. They obtained uniform values that averaged 1.1 HFU (1 HFU=$^{-6}$cal/cm^2 sec). Decker (1969) presented nine heat flow values in Colorado and New Mexico. He suggested that the high and variable heat flow of the Southern Rocky Mountains might be due to radioactivity in the crust and that the high heat flux in the Basin and Range of southern New Mexico might be related to sources other than crustal radioactivity. Roy and others (1968) presented six additional sites in New Mexico supporting the concept of high heat flow in the Basin and Range. Sass and others (1971a) presented heat flow sites in the western United States; one unreduced site was in the New Mexico-southern Colorado area. Reiter and others (1975) showed that the western

portion of the Rio Grande rift in New Mexico and southern Colorado has anomalously high heat flows (>2.5 HFU) and that the geothermal character of the eastern Colorado Plateau is quite complex. Decker and Smithson (1975) also showed that the Rio Grande rift in southern New Mexico has high heat flow.

PRESENTATION OF HEAT FLOW DATA

Table 1 summarizes the heat flow data at 55 sites in northern New Mexico and southern Colorado. The heat flow values are also given on the map in figure 2 near the dot identifying the location of the drill sites. The heat flows are calculated by multiplying linear thermal gradients by their corresponding average thermal conductivities. Appendix I gives the experimental procedure used in measuring thermal gradients and thermal conductivities. A best heat flow value for each well is normally chosen by averaging the heat fluxes in different linear gradient zones throughout the well. However, if the heat fluxes vary substantially in a borehole, then we attempt to choose the fluxes that seem reasonable in light of the conductivity control, the linearity of the gradient, possible regional groundwater movement, or vertical movement of water within the well bore.

The heat flow measurements are evaluated using the criteria of Reiter and others (1975). For example, "A" measurements are thought to be within ±10%, "B" measurements, within ±20%, and "C" measurements have an uncertainty greater than ±20%. "A" measurements typically are made in boreholes 300 m and deeper in which there is good thermal conductivity control. Generally "A" heat flow measurements have constant thermal gradient zones of 100 m and longer. "B" measurements normally have shorter constant thermal

TABLE I SUMMARY OF HEAT FLOW DATA

LOCALITY	NORTH LAT	WEST LONG	ELEV METERS	DEPTH INTERVAL METERS	THERMAL GRADIENT DEG.C/KM	N	TYPE OF SAMPLE**	THERMAL CONDUCTIVITY MCAL/CM-SEC-DEG.C	HEAT FLOW HFU@	BEST HEAT FLOW ESTIMATE HFU@	QUALITY OF HEAT FL VALUE
[illegible]OF/EAST (NM)	36 16	104 06	1878	130-410	25.35±0.19	22	FRAGMENTS	6.04±0.19	1.53±0.06	1.53	A
[illegible]OF/NORTH (NM)	36 24	104 14	2012	230-470	27.56±0.10	61	FRAGMENTS	5.89±0.40	1.62±0.12	1.62	A
[illegible] CREEK (C)	37 25	106 30	3201	60-160	30.89±0.27	8	FRAGMENTS	7.09±0.44	2.19±0.16	2.20	B
[illegible]YO TETILLA (NM)	35 40	106 11	2050	100-180	48.89±1.13	10	FRAGMENTS	5.32±0.49	2.60±0.31	2.60	C
[illegible] CROW CR (NM)	36 47	104 42	2439	90-325	36.19±0.30	12	FRAGMENTS	6.70±0.30	2.42±0.13	2.42	B
[illegible]WATER(NM)	35 15	107 59	2195	20-110	18.90±0.49	7	FRAGMENTS	7.65±0.33	1.45±0.10	1.44	C
[illegible]MAN #2 (NM)	35 53	106 09	1800	190-220	33.94±2.32	8	FRAGMENTS	5.11±0.09	1.73±0.15	1.73	C
[illegible]ON CITY EMBYMT (C)	38 13	105 01	2134	100-170#	36.22±1.02	3	FRAGMENTS	5.62±0.17	2.04±0.12	2.04	C
[illegible]ZO (NM)	34 48	107 08	1886	50-350	24.84±0.33	10	FRAGMENTS	5.77±0.31	1.43±0.10	1.96	A
				350-820	35.91±0.11	14	FRAGMENTS	5.46±0.15	1.96±0.06		
[illegible]LLA (NM)	36 32	106 29	2317	20-190	31.28±0.34	8	FRAGMENTS	5.62±0.19	1.76±0.08	1.83	A
				300-340	39.20±0.46	7	FRAGMENTS	4.81±0.09	1.89±0.06		
[illegible]ILLOS #1 (NM)	35 27	106 06	1866	70-150	24.06±0.20	13	FRAGMENTS	4.99±0.14	1.20±0.04	1.20	C
[illegible]ILLOS #2 (NM)	35 27	106 06	1884	80-129	26.39±0.40	9	FRAGMENTS	4.98±0.19	1.31±0.07	1.31	C
[illegible]ILLOS #3 (NM)	35 27	106 07	1829	80-184	24.86±0.15	13	FRAGMENTS	4.92±0.14	1.22±0.04	1.22	B
[illegible]PELL SPADE (NM)	35 16	103 51	1223	150-340	26.50±0.33	16	FRAGMENTS	5.25±0.19	1.39±0.07	1.40	A
				500-900	18.16±0.18	16	FRAGMENTS	7.61±0.23	1.38±0.06		
				940-1400	26.39±0.20	11	FRAGMENTS	5.40±0.19	1.43±0.06		
[illegible]NEY CREEK (NM)	36 55	104 52	2439	120-260	64.38±1.06	8	FRAGMENTS	5.14±0.11	3.31±0.13	2.88	B
				370-480	38.46±0.95	42	FRAGMENTS	6.37±0.13	2.45±0.11		
[illegible]OR/WEST (NM)	36 13	104 41	1826	80-170	44.84±0.34	8	FRAGMENTS*	6.23±0.60	2.79±0.29	2.87	A
				220-300	53.02±0.79	5	FRAGMENTS*	5.56±0.11	2.95±0.10		
[illegible]ON #2 (NM)	36 13	105 48	2270	40-160	33.74±0.66	7	CORE	14.69±0.33	4.96±0.21	5.47	C
[illegible]UEN #1 (NM)	35 16	106 12	2037	80-150	27.44±0.27	4	CORE	9.29±0.26	2.55±0.10	1.24	C
				150-250	18.83±0.20	5	CORE	6.56±0.40	1.24±0.09		
[illegible]NEROS RD (C)	37 56	104 49	1857	30-110	19.81±0.68	6	FRAGMENTS*	10.46±0.22	2.07±0.12	2.07	C
[illegible]RSON # 6 (C)	38 10	104 47	1524	60-180	45.93±0.40	5	FRAGMENTS*	4.99±0.07	2.29±0.05	2.41	B
				210-290	23.38±0.58	5	FRAGMENTS*	10.84±0.28	2.53±0.13		
[illegible] JUNTA/NORTH (C)	38 01	103 32	1250	50-130	40.80±0.59	6	FRAGMENTS	5.46±0.17	2.23±0.10	2.23	C
[illegible]S VEGAS #1 (NM)	35 35	105 15	1989	80-150#	17.78±0.48	4	FRAGMENTS	5.62±0.19	1.00±0.06	1.50	C
				150-198	27.25±0.52	3	FRAGMENTS	5.50±0.40	1.50±0.14		
[illegible]S VEGAS #2 (NM)	35 34	105 15	1951	100-170	22.51±0.44	9	FRAGMENTS	6.45±0.68	1.45±0.18	1.45	B
[illegible]TLE BEAR MTN (NM)	34 17	107 15	1902	60-210#	20.13±0.58	6	FRAGMENTS	7.04±0.28	1.42±0.10	1.72	C
				200-290	29.15±0.36	7	FRAGMENTS	5.90±0.12	1.72±0.06		
[illegible]TLE CROW CR (NM)	36 49	104 41	2439	110-225	38.31±0.46	5	FRAGMENTS	5.56±0.57	2.13±0.25	2.13	B
[illegible]S (NM)	36 09	104 42	1372	20-90	36.12±0.44	9	FRAGMENTS	6.32±0.62	2.28±0.25	2.35	C
				90-170	43.15±0.25	5	FRAGMENTS	5.66±0.08	2.44±0.05		
[illegible]ORA (NM)	36 28	103 36	1788	190-290	20.74±0.88	8	FRAGMENTS	7.93±0.61	1.64±0.20	1.30	B
[illegible]GY CR/SE (C)	38 58	104 53	1924	60-100#	30.85±1.17	8	FRAGMENTS	5.25±0.15	1.62±0.11	1.93	C
				115-180	36.84±0.71	8	FRAGMENTS	5.25±0.15	1.93±0.09		
[illegible]A/EAST (NM)	36 09	104 35	1921	80-140	43.37±0.29	8	FRAGMENTS*	6.23±0.60	2.70±0.28	2.75	C
				140-180	55.31±1.11	5	FRAGMENTS*	5.06±0.20	2.80±0.17		
[illegible]A/NW (NM)	36 11	104 40	1861	80-170	43.17±0.17	8	FRAGMENTS*	6.23±0.60	2.69±0.27	2.98	C
				170-240	64.62±0.80	5	FRAGMENTS*	5.06±0.20	3.27±0.17		
[illegible]IZ MTN 2 (NM)	35 19	106 10	2399	140-720	18.18±0.11	26	CORE	7.32±0.29	1.33±0.06	1.33	A
[illegible]IZ MTN 3 (NM)	35 18	106 10	2218	130-280	16.03±0.13	7	CORE	7.82±0.77	1.25±0.13	1.33	B
				370-420	22.00±0.39	3	CORE	6.36±0.10	1.40±0.05		
[illegible]RO CANYON (NM)	36 53	104 43	2409	40-160	38.08±0.73	8	FRAGMENTS	7.02±0.33	2.67±0.18	2.69	A
				160-280	50.58±0.92	5	FRAGMENTS	5.35±0.04	2.71±0.07		
[illegible]RLO/SOUTH (C)	38 11	104 44	1570	80-130	51.69±1.13	5	FRAGMENTS*	5.15±0.57	2.66±0.36	2.69	C
				130-200	25.31±1.10	5	FRAGMENTS*	10.71±0.23	2.71±0.18		
[illegible]RLO/WEST (C)	38 18	104 46	1524	80-190	51.77±0.70	5	FRAGMENTS*	5.15±0.57	2.67±0.34	2.85	C
				190-240	30.36±1.17	5	FRAGMENTS*	10.71±0.23	3.25±0.20		
[illegible]STA #2 (NM)	36 42	105 31	2933	310-450	18.52±0.17	2	CORE	9.25±1.08	1.71±0.22	1.74	A
				450-590	22.70±0.13	4	CORE	7.77±0.26	1.76±0.07		
				590-690	21.22±0.32	7	CORE	8.19±0.34	1.74±0.10		
[illegible]STA # 3 (NM)	36 42	105 32	2900	310-410	20.32±0.16	2	CORE	9.25±1.08	1.88±0.24	1.81	C
				430-510	23.32±0.30	4	CORE	7.77±0.26	1.81±0.08		
				510-590	21.21±0.41	7	CORE	8.19±0.34	1.74±0.11		
[illegible]S CREEK (C)	38 14	105 00	2134	50-150	22.14±0.41	4	FRAGMENTS	10.84±0.28	2.40±0.11	2.40	C
[illegible]S LUCHARAS (C)	37 32	104 54	2104	100-240	31.91±0.38	7	FRAGMENTS*	6.09±0.13	1.94±0.07	1.97	B
				290-450	34.62±0.20	11	FRAGMENTS*	5.76±0.31	1.99±0.12		
[illegible]S CRISTOBAL (NM)	36 38	105 39	2317	140-290	35.52±0.59	20	FRAGMENTS	8.79±0.15	3.12±0.11	3.12	A
[illegible]S PEDRO 4 (NM)	35 15	106 11	2165	190-410	22.74±0.15	1	FRAGMENTS	6.26±1.56	1.42±0.37	1.42	A
[illegible]PLE (NM)	36 31	104 22	2013	120-330	30.69±0.25	14	FRAGMENTS	7.96±0.43	2.44±0.15	2.44	A
[illegible]LE HILLS/NE (C)	37 46	103 37	1372	50-100	32.70±0.70	6	FRAGMENTS	4.79±0.13	1.57±0.08	1.90	C
				100-145	46.36±0.84	6	FRAGMENTS	4.79±0.13	2.22±0.10		
[illegible]RA DEL OJITO (C)	37 16	105 14	2363	250-350	64.20±0.35	8	FRAGMENTS	4.03±0.17	2.57±0.12	2.51	A
				350-470	58.30±0.37	7	FRAGMENTS	4.17±0.05	2.43±0.04		
[illegible]OAM ROAD (C)	38 14	104 56	2134	105-135	38.74±0.59	5	FRAGMENTS*	5.15±0.57	2.00±0.25	2.00	C
[illegible]MS (NM)	36 08	104 43	1927	90-206	43.62±0.34	6	FRAGMENTS	6.13±0.12	2.67±0.07	2.71	B
[illegible]ORRO/S (NM)	33 57	106 56	1555	40-100#	21.79±0.34	7	FRAGMENTS	5.03±0.40	1.13±0.11	1.73	C
				110-150	34.49±0.97	7	FRAGMENTS	5.03±0.40	1.73±0.19		
[illegible]TILLA PEAK (NM)	35 35	106 13	1889	70-140	39.57±0.46	10	FRAGMENTS	5.06±0.41	2.00±0.19	2.00	C
[illegible]S MONTOSA (NM)	34 05	107 22	2098	90-200	34.56±0.51	3	FRAGMENTS	4.98±0.07	1.72±0.05	1.96	C
				200-240	44.79±0.53	2	FRAGMENTS	4.91±0.39	2.35±0.20		
[illegible]OUISE MTN 1 (NM)	35 30	106 06	1918	40-120	28.14±0.34	8	CORE	4.70±0.05	1.32±0.03	1.32	C
[illegible]OUISE MTN 2 (NM)	35 31	106 07	1918	60-110#	21.21±0.86	5	CORE	4.70±0.06	1.01±0.05	1.22	C
				110-160	23.68±0.21	6	CORE	5.15±0.29	1.22±0.08		
[illegible] BREMMER CR (NM)	36 48	104 57	2323	130-250	52.68±0.43	6	FRAGMENTS	4.14±0.23	2.13±0.14	2.04	A
				270-500	37.25±0.20	7	FRAGMENTS	5.11±0.15	1.90±0.07		
[illegible]ES (NM)	36 08	103 54	1720	90-430	25.29±0.30	24	FRAGMENTS	5.69±0.30	1.44±0.09	1.44	A

[illegible]S NUMBER OF THERMAL CONDUCTIVITY SAMPLES
1 HFU = 1 UCAL/CM*CM-SEC
[illegible] CONDUCTIVITIES OF FRAGMENT SAMPLES HAVE BEEN CORRECTED FOR POROSITY
OUTCROP SAMPLES
THIS DEPTH INTERVAL NOT USED IN DETERMINING BEST HEAT FLOW ESTIMATE
INDICATES THE STANDARD DEVIATION
[illegible], SITE IN COLORADO; (NM), SITE IN NEW MEXICO
[illegible]ATIONS ARE ± 20 METERS

gradient zones, 40-90 m or poor thermal conductivity control. "C" measurements generally indicate poor conductivity control (perhaps outcrop samples) and disturbances in the temperature log.

Figure 2 shows the major basins and uplifts in northern New Mexico and southern Colorado. The hatched areas show regions of extensive volcanic activity. High heat flow values were observed in the San Juan volcanic area (2.2-3.4 HFU) and in the Jemez volcanic field (>3.0 HFU). Somewhat lower heat flow values were observed in the Mount Taylor volcanic field (1.5-2.0 HFU). Normal heat flow values were observed in the Raton, Clayton, and Capulin volcanic fields (1.3-1.5 HFU).

In northwestern New Mexico and southwestern Colorado the San Juan and Blanding basins exhibit normal heat flows (1.3-1.5 HFU). However, in northeastern New Mexico and southeastern Colorado the Las Vegas and Raton basins have higher heat flows (≥2.0 HFU). In east central New Mexico the Tucumcari basin has a normal heat flow (1.4 HFU).

Figure 3 shows a heat flow contour map of northern New Mexico and southern Colorado. In northeastern New Mexico and southeastern Colorado this map is a refinement of a previous heat flow map published by Reiter and others (1975). The contour interval is 0.5 HFU. The contour intervals are shaded light to dark with the lightest areas ≤1.5 HFU and the darkest areas ≥2.5 HFU. The contours

Figure 2. Heat flow sites in northern New Mexico and southern Colorado. Data in parenthesis from Reiter and others (1975). Data in brackets from Decker (1969) and from Sass and others (1971a). Base map adapted from A.A.P.G. tectonic map (1962).

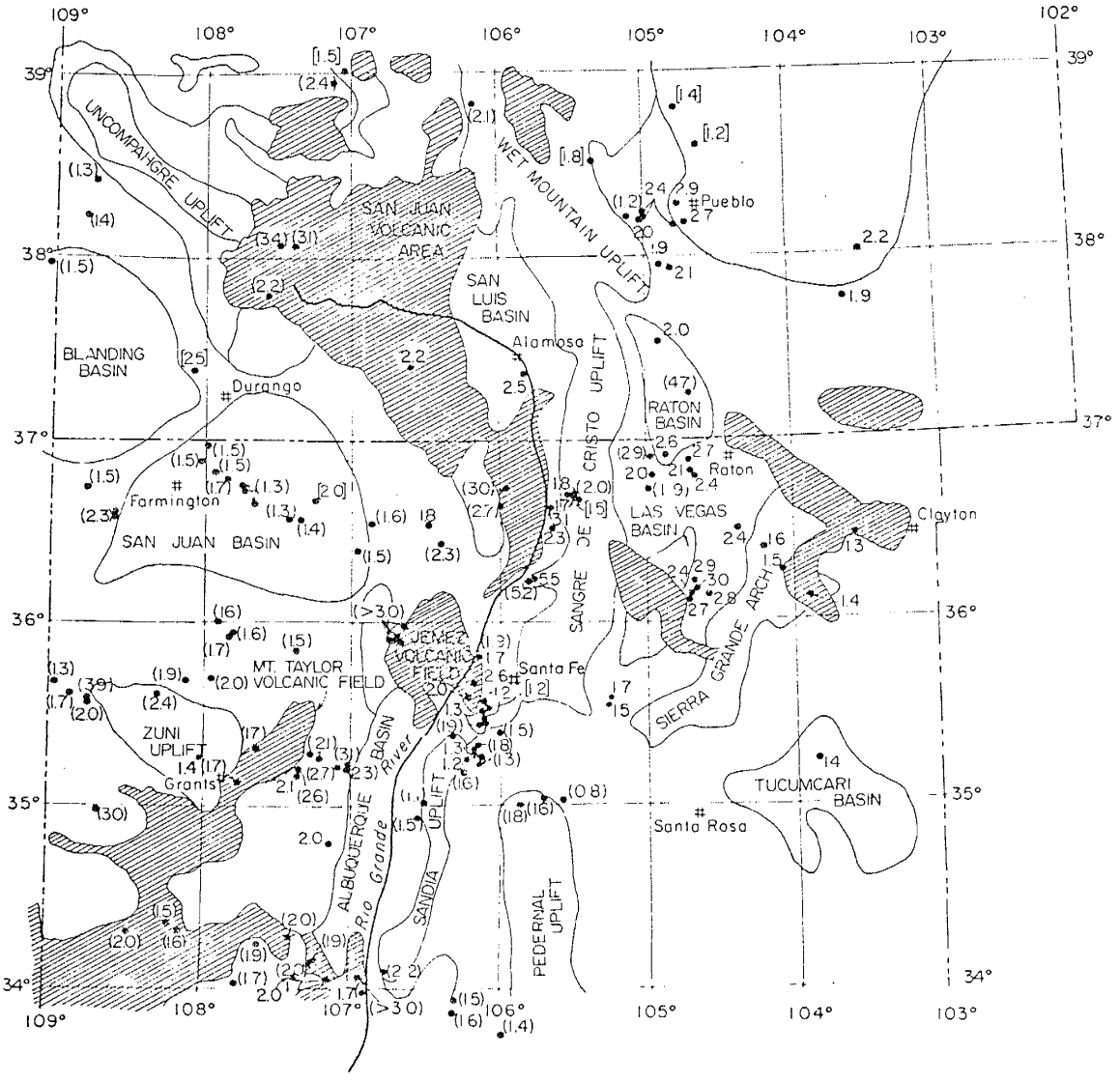

Figure 3. Terrestrial heat flow contour map of northern New Mexico and southern Colorado. Contour interval, 0.5 HFU. Plus signs indicate control sites measured by New Mexico Institute of Mining and Technology; Xs indicate control sites measured by other investigators.

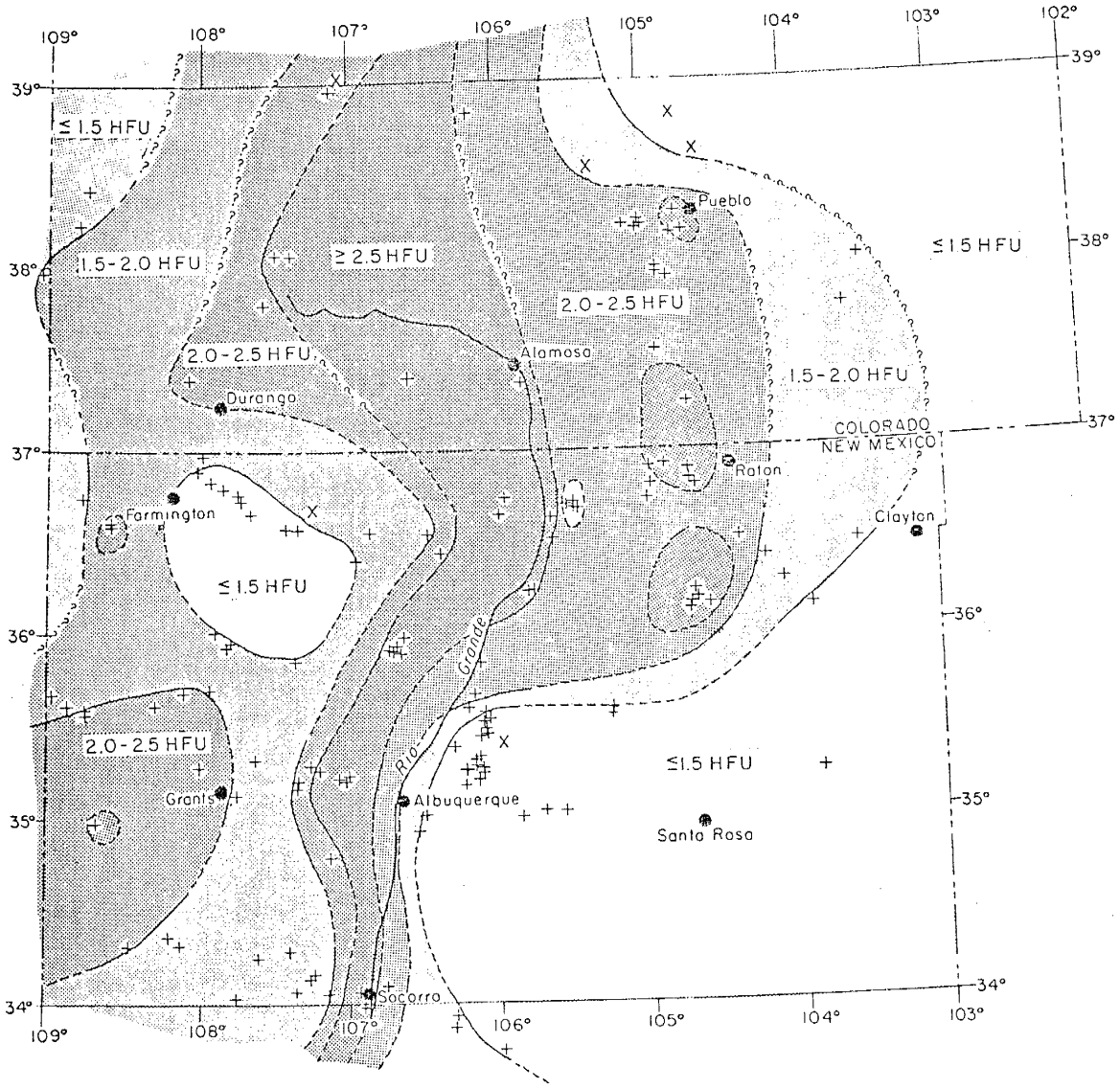

are based on the magnitude, quality, and compatibility of heat flow measurements within a region. The contours are solid lines in areas where there is good control; that is, it appears unlikely that additional data will change the character and location of the contours. Dashed contours indicate that additional data may change the location of the contours but probably not the character. Question marks are used where data coverage is sparse and considerable ambiguity exists in the location and character of the contours.

A broad heat flow anomaly in northern New Mexico and southern Colorado associated with the Southern Rocky Mountain complex, contrasts with a narrow heat flow anomaly between Santa Fe and Socorro, New Mexico, apparently associated only with the Rio Grande rift. Between Santa Fe, New Mexico, and Pueblo, Colorado, the change from heat flow values of $\geq$2.5 HFU observed near the Rio Grande rift to heat flow values of $\leq$1.5 HFU observed on the Great Plains occurs over a distance of 200 to 300 km. However, between Santa Fe and Socorro, New Mexico, the change from heat flow values of $\geq$2.5 HFU to heat flow values of $\leq$1.5 HFU occurs over a distance of 20 to 30 km. Present data suggest that the heat flow pattern between Santa Fe and Pueblo is more complex, demonstrating local anomalies within the broad regional anomaly - for example in proximity to the Las Vegas basin, the Raton basin, near Pueblo, Colorado, and near Questa, New Mexico. More data will be necessary

to determine the size and character of these anomalies.

The Great Plains has been considered an area of low to normal heat flow (≤1.5 HFU) - for example, observed data in southeastern New Mexico have a mean heat flow of 1.1 HFU (Herrin and Clark, 1956). This characterization does not appear to be valid in northeastern New Mexico and southeastern Colorado where the heat fluxes vary from 1.3 to over 2.5 HFU.

PRESENTATION OF RADIOGENIC DATA

Birch and others (1968), Roy and others (1968) and Lachenbruch (1968) describe a linear relation between heat flow and the radiogenic heat production of surface plutonic rocks. The relation may be written

$$q = q^* + D\,A(o) \qquad \text{(equation 1)}$$

where q is the near surface heat flow, A(o) is the radioactive heat generation of surface plutonic rocks, and q* and D are constants characteristic of large geologic provinces (Roy and others, 1968). Birch and others (1968) and Roy and others (1968) identify q* as the constant heat flow into the base of a crustal layer of thickness D. Most of the heat due to radioactive decay is generated between the surface and depth D. Lachenbruch (1970) argues that the radioactive source distribution in the crust must decrease exponentially with depth, that is

$$A(z) = A(o)e^{-Z/D} \qquad \text{(equation 2)}$$

As a result, q* becomes the heat flux through the base of some crustal layer, of variable thickness z*, defined such that the heat production, $A(o)e^{-Z^*/D}$, is constant. If the heat production below z* is negligible, then q* is the heat flux from the mantle.

Reduced heat flow values, q*, are calculated by transposing equation 1,

$$q^* = q - D\,A(o) \qquad \text{(equation 3)}$$

when q us the best estimate of the near surface heat flow

in HFU (10^{-6} calories/cm^2 sec), A(o) is the measured heat generation in HGU (10^{-13} calories/cm^3 sec), and D is the slope in centimeters of the linear heat flow relation, equation 1, determined by Roy and others (1968) for the area. Within the United States Roy and others (1968) identify three heat flow provinces: the eastern United States, where q*=0.8 HFU and D=8.5 km; the Basin and Range province, where q*=1.4 HFU and D=9.4 km; the Sierra Nevada, where q*=0.4 HFU and D=10 km. A slope of 10 km is used in all of the reduced heat flow calculations in the area by Roy and others (1968), Decker and Smithson (1975), and this manuscript.

Figure 4 shows the locations of reduced heat flow sites in New Mexico and southern Colorado. Heat generation due to potassium, uranium, and thorium was measured in three general areas: 1) within the Southern Rocky Mountain complex of northern New Mexico and southern Colorado, 2) east of the Rio Grande rift between Santa Fe and Socorro, New Mexico, 3) along the Rio Grande rift from Socorro south to the border with Mexico. The reduced heat flows and associated radioactivity data are presented in Table 2. The technique employed to make these measurements is explained in Appendix III.

Within the Southern Rocky Mountain region the reduced heat flows at Los Alamos (>3.2 HFU) and at Ruby Mountain (2.1 HFU) are higher than the intercept q* predicted by Roy and others (1968) for the region (1.3-1.4 HFU). However,

Figure 4. Reduced heat flow sites in New Mexico and southern Colorado. Data in parenthesis from Decker (1975). Other data presented in this manuscript. Base map adapted from A.A.P.G. geologic highway map (1962).

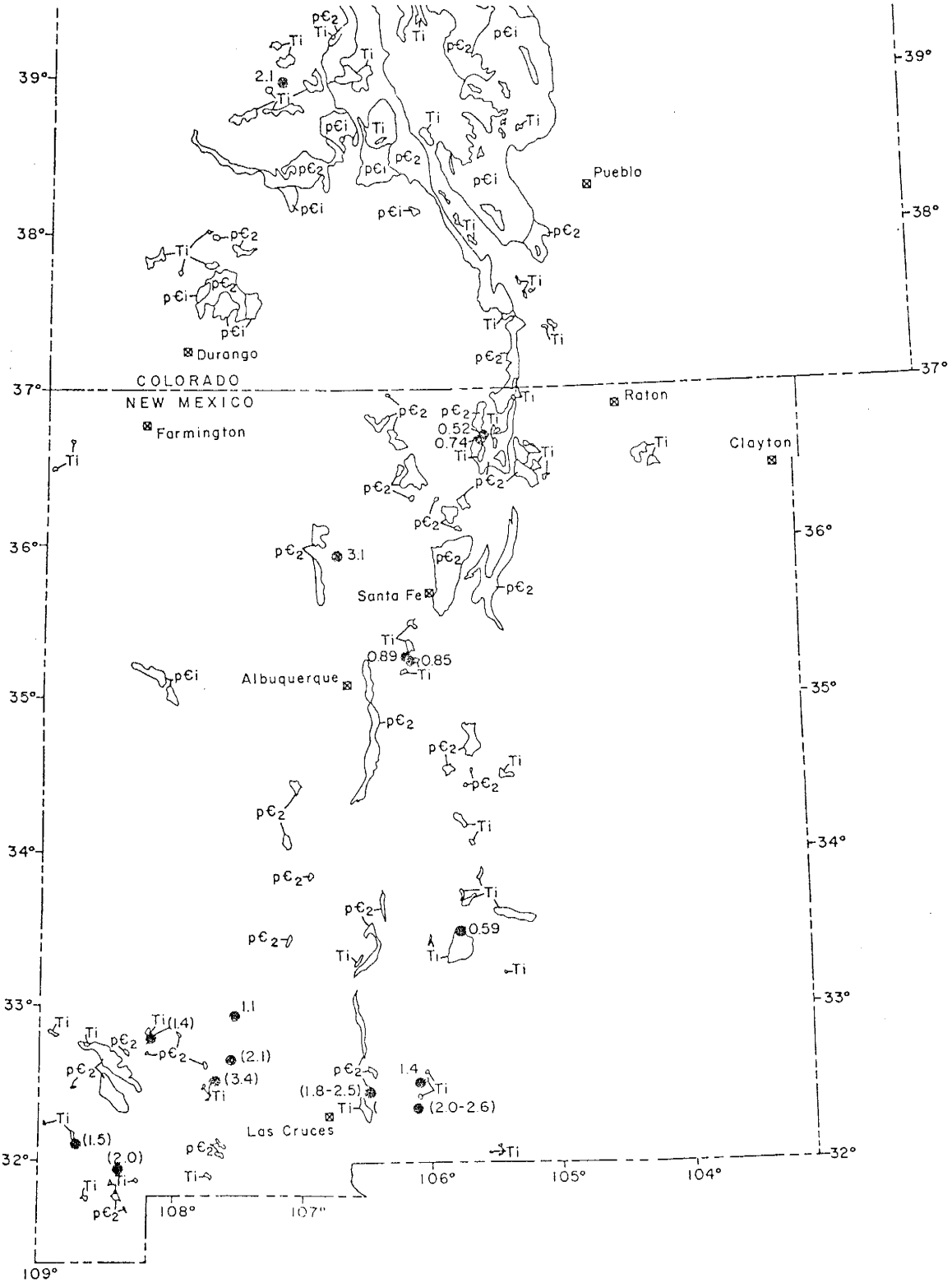

Table 2. Summary of Radioactivity and Reduced Heat Flow Data

Well Name	Rock Type	No. of Samples	Potassium (%)	Uranium (ppm)	Thorium (ppm)	Heat Generation (HGU)	Reduced Heat Flow (HFU)
Ruby Mountain[+]	Monzonite	5	4.10±.20	1.95± .15	5.41± .51	3.05	2.10
Questa #1[+]	Granite	3	0.78±.55	13.02±2.01	31.71± .57	12.85	0.52
Questa #2	Granite	5	1.49±.24	13.61±1.23	25.07±1.43	12.97	0.74
Los Alamos*	Granite	4	3.52±.17	0.92± .39	15.95±3.23	3.09	>3.20
San Pedro #3[+]	Monzonite	6	2.55±.18	2.51± .30	10.95± .80	3.98	0.89
San Pedro #4	Monzonite	4	3.33±.11	3.39± .07	12.02± .24	4.88	0.85
Sierra Blanca[+]	Monzonite	4	3.36±.63	9.97±3.24	28.65±6.78	11.76	0.59
Animas Peak[+]	Granite	5	3.96±.20	5.18± .33	14.50± .58	6.55	1.05
Orogrande[+]	Granodiorite	6	3.18±.31	1.96± .20	7.37± .25	3.18	1.43

[+]unreduced heat flows from Reiter and others (1975).

* " " " " " " " (in prep.).

the reduced heat flow values at Questa (0.52 and 0.74 HFU) are lower than the intercept predicted by Roy and others (1968). East of the Rio Grande rift between Santa Fe and Socorro, New Mexico, the reduced heat flow values at San Pedro (0.89 and 0.85 HFU) compare closely with the 0.8±.1 HFU intercept for the Great Plains as suggested by Roy and others (1968) and Decker and Smithson (1975).

East of the Rio Grande rift in southern New Mexico, the reduced heat flow value at Sierra Blanca (0.59 HFU) is intermediate between the Great Plains and the Sierra Nevada reduced heat flow values. The reduced heat flow value at Animas Peak (1.1 HFU) is intermediate between Basin and Range and Great Plains values. A reduced heat flow of 1.4 HFU, a typical Basin and Range value, was measured in the southern region near Orogrande. The reduced value differs substantially from the value of 2.0-2.6 HFU that Decker and Smithson (1975) measured about 15 km to the south.

Figure 5 shows a plot of the heat flow versus heat generation for the Rio Grande rift and vicinity of New Mexico and southern Colorado. The solid line represents the linear heat flow relation between unreduced heat flow and near surface radioactive heat generation for the Basin and Range (Roy and others, 1968). Of the 19 values plotted, only four, Lordsburg, Santa Rita, Orogrande/North, and Animas Peak plot within ±20% of this linear relation. The vertical dashed line, representing a crustal heat production of 3.8

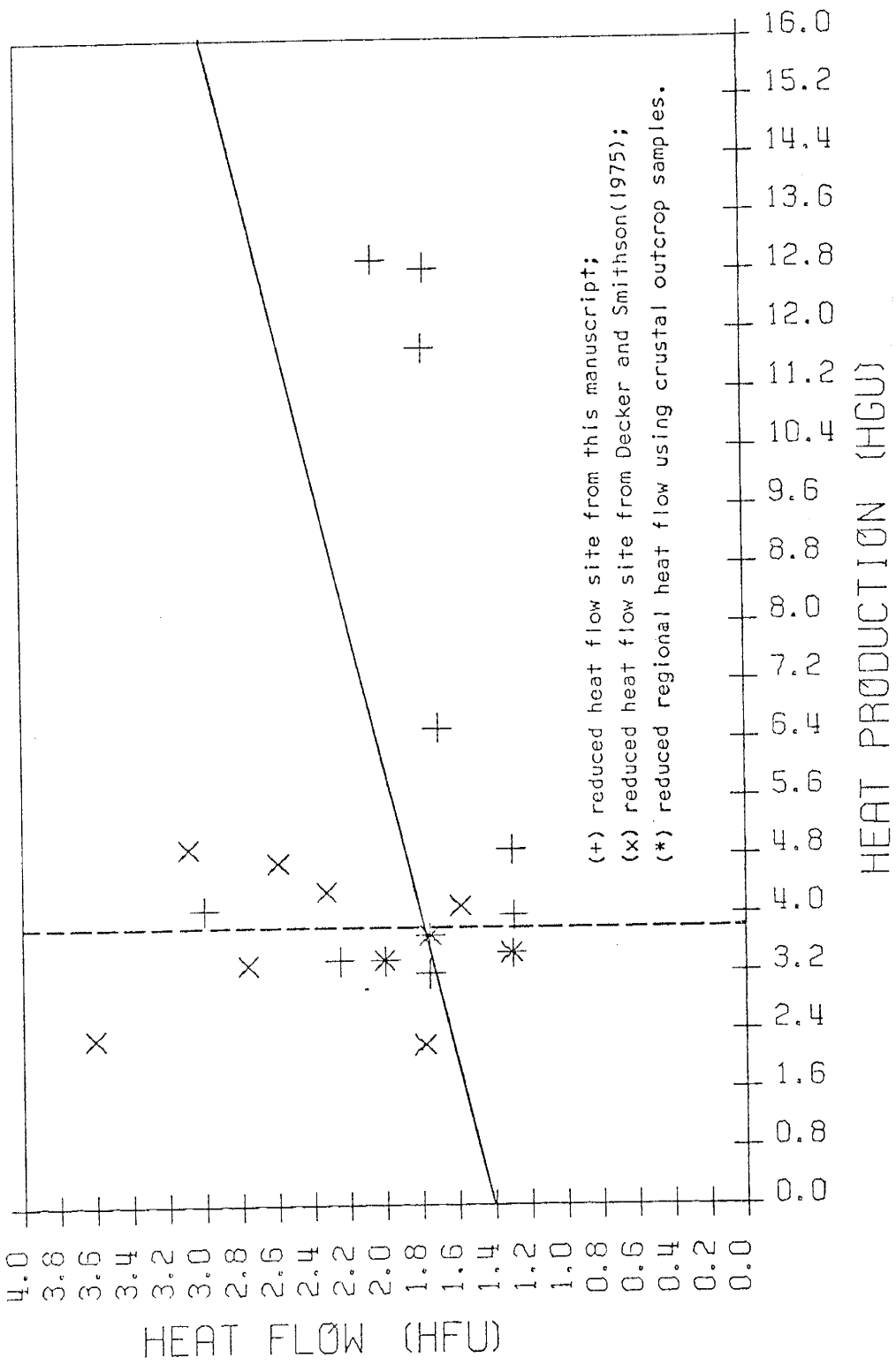

FIGURE 5 HEAT FLOW VERSUS HEAT PRODUCTION

HGU is the average heat generation of all sites measured in this study except Questa and Sierra Blanca, where the data plotted more than two standard deviations from the mean. This implies that the radioactive heat generation in the Rio Grande rift vicinity is relatively constant with about 0.4 HFU of the unreduced heat flow coming from radioactive decay in the upper crust.

Most of the core samples counted are from Tertiary or Laramide intrusives. To investigate the probability that these core samples are representative of the upper crust in the area of investigation, three additional composite outcrop samples were measured. Dr. Kent C. Condie supplied the composite samples based on extensive field work in New Mexico. The composition of the three samples is given in Table 3. The results of the radioactivity measurements are presented in Table 4. The northern composite sample represents a best estimate of the upper crust in the Southern Rocky Mountain complex of northern New Mexico and southern Colorado, the central one a best estimate of the upper crust in the eastern part of the Rio Grande rift between Santa Fe and Socorro, the southern one a best estimate of the upper crust in the Rio Grande rift vicinity of south central New Mexico. The heat generation is essentially constant in the three composite samples (the mean heat production of the three samples is 3.5 HGU). It appears that along the Rio Grande rift the average heat generation obtained for the composite crustal samples (3.5 HFU) is only slightly lower than the average for core

samples (3.8 HGU). For the area of investigation, it appears that core samples from intrusives yield samples representative of the upper crust.

Table 3. Composition of three regional average samples.

Region	Granite (%)	Quartzite (%)	Siliceous Volcanics (%)	Amphibolite (%)	Mica Schist Phyllite (%)
North Composite Sample	60	15	10	5	10
Central Composite Sample	40	15	15	5	25
South Composite Sample	70	10	0	10	10

Table 4. Summary of radioactivity data for composite crustal samples

Name of Well	# Samples	Potassium (%)	Uranium (ppm)	Thorium (ppm)	Heat Generation (HGU)
North Composite Sample	1	3.67	1.10	10.95	3.36
Central Composite Sample	1	3.32	1.66	9.91	3.46
South Composite Sample	1	3.01	1.69	11.70	3.70

DISCUSSION

The Southern Rocky Mountain complex in northern New Mexico and southern Colorado is characterized by a broad area of high heat flow with very high heat flows along the Rio Grande rift. The broad high heat flow region dramatically narrows between Santa Fe and Socorro, New Mexico. This geothermal pattern suggests deep and broadly distributed thermal sources under the Southern Rocky Mountain complex of northern New Mexico and southern Colorado as opposed to shallow and narrowly distributed thermal sources along the Rio Grande rift between Santa Fe and Socorro. It appears from the contour map (figure 3) that the half-width of the thermal anomaly associated with the Southern Rocky Mountain complex in northern New Mexico and southern Colorado is approximately an order of magnitude greater than the half-width of the thermal anomaly associated only with the Rio Grande rift between Santa Fe and Socorro. This suggests considerably deeper thermal sources for the Southern Rocky Mountain anomaly as compared to the Rio Grande rift anomaly. If the depth of thermal sources within the Rio Grande rift are of the order of 15-30 km as suggested by the data of Lipman (1969) and Sanford (1973), then the depth to the thermal sources associated with the Southern Rocky Mountain anomaly should be of the order of 150-300 km, which is compatable with the data of Schmucker (1970).

The broad heat flow anomaly associated with the Southern Rocky Mountains extends onto the Great Plains in northeastern New Mexico and southeastern Colorado. Caner and others (1967) describe a geomagnetic discontinuity which has the same character as the heat flow anomaly in New Mexico and southern Colorado. Schmucker (1970) postulates that the geomagnetic anomaly underneath the Southern Rocky Mountains is caused by an increase of 100°C at a depth of 50-300 km. This may suggest that the higher mantle temperatures postulated for the Southern Rocky Mountains are the sources of high heat flows that extend onto the Great Plains of northeastern New Mexico and southeastern Colorado.

In northern New Mexico and southern Colorado within the Rio Grande rift, the volcanic rocks are primarily thoeleiitic basalts probably fractionating at a depth of 15-20 km (Lipman, 1969; Lipman and others, 1973). Lipman (1969) suggested that the Rio Grande rift may have been an area of high heat flow and that possibly an upwarp in the mantle underneath the rift allowed the fractionation of basalt to take place at an unusually high crustal level. This area is characterized by unreduced heat flows greater than 2.5 HFU, supporting Lipman's hypothesis (figure 2 and figure 3).

The volcanic rocks in San Juan volcanic area of southwestern Colorado are primarily made up of equal amounts of andesitic and rhyolitic rocks erupting from a cluster of central vent volcanoes (Eardley, 1962; Lipman and others,

1973). The western and central portions of the San Juan volcanic area contain abundant cauldron subsidence structures and abundant ash-flow deposits (Luedke and Burbank, 1968, Steven and Epis, 1968). The San Juan volcanic area has high heat flow (2.2-3.4 HFU) but the values are not as consistently high as those within the Rio Grande rift (Reiter and others, 1975, new data this manuscript). Heat flow values of 3.4 and 3.1 HFU are reported by Reiter and others (1975) within the Lake City caldera. The Mount Taylor volcanic field in north-central New Mexico is the result of a large central vent type volcano. The Jemez volcanic area in north central New Mexico is the result of multiple eruptions which have produced a cauldron structure. The rocks in both areas are primarily rhyolitic tuffs, latites, and porphyritic andesites (Lipman and others, 1973). The heat fluxes range from 1.5-2.0 HFU in the Mount Taylor volcanic field and from 1.7 to >3.0 HFU in the Jemez volcanic field. The higher heat fluxes in the Jemez and San Juan areas may reflect the existence of large caldera-type volcanic centers with considerably larger magmatic plumbing systems than the central vent volcano of Mount Taylor (Chapin, personal communication).

The anomalously high heat flows in the Las Vegas and Raton Basins contrast with low to normal heat flows in other basins in the region, the San Juan, the Blanding and the Tucumcari basins. The Las Vegas and Raton Basins have been extensively intruded by igneous rocks (Johnson

and others, 1966; Johnson, 1968). The Tucumcari basin in the Great Plains of eastern New Mexico, and the San Juan and Blanding Basins within the Colorado Plateau have had little igneous or volcanic activity (Eardley, 1962).

The results of the crustal radiogenic measurements in the Rio Grande rift vicinity (this manuscript; Decker and Smithson, 1975) show that radioactive decay in the crust contributes regionally 0.38±.03 HFU to the unreduced heat flow within the area (figure 5). This implies that the heat flow anomalies observed in New Mexico and southern Colorado along the Rio Grande rift, (this study; Reiter and others, 1975; Decker and Smithson, 1975) are not caused by lateral variations in the concentrations of potassium, uranium and thorium within the crust. The Rio Grande rift high heat flow anomaly observed by Decker and Smithson (1975) in southern New Mexico and by Reiter and others (1975) throughout New Mexico and southern Colorado is probably a reflection of non-radioactive thermal sources underneath the Rio Grande depression.

Reiter and others (1975) suggest an extensive fracture system with magmatic intrusions as a possible thermal source under the Rio Grande rift. Chapin (1971) proposes a thinning of the crust and an upward bulge in the mantle under the Rio Grande rift. The sharp narrow high heat flow anomaly along the Rio Grande rift between Santa Fe and Socorro suggests a shallow thermal source in this area. Lipman (1969) suggests that fractionation in the crust at shallow depths (15-20 km) is necessary to produce the uncontaminated

theoleiitic basalts that have erupted within the Rio Grande rift. Sanford and others (1973) have identified a sharp discontinuity, possibly underlain by material of low rigidity at a depth of 18 km near Socorro dipping to a depth of 30 km, 60 km north of Socorro. These heat flow, geochemical, and seismic data imply that the thermal source of the Rio Grande rift anomaly in northern New Mexico may be quite shallow.

If the heat flow contributions due to volcanic and tectonic sources within the crust and upper mantle, along the Rio Grande rift, could be estimated and subtracted from the surface heat flows, the resulting heat flow values and their appropriate heat generation values may possibly plot along the line representing the linear heat flow relation of Roy and others (1972) for the Basin and Range and the southern Rocky Mountains. However, changes in heat flow due to these small variations in crustal radioactive heat generation would be very difficult to measure. Even though the heat flow-heat generation values along the Rio Grande rift do not plot on the line defined by the linear heat flow relation for the Basin and Range, a slope of 10 km is used for the reduced heat flow calculations in this manuscript. The range of slopes observed for the linear heat flow relation in the United States is 7.5 to 10 km with slopes for the Rocky Mountains and the Basin and Range being almost identical. Consequently, with present data, it would appear reasonable to use a slope of 10 km for reduced

heat flow measurements in the vicinity of the Rio Grande rift. The low reduced heat flow values at Questa, .52 and .74 HFU, are below the 1.4 HFU intercept of the Southern Rocky Mountains-Basin and Range heat flow province. The reduced heat flow value of .59 HFU at Sierra Blanca is below the 0.8 HFU intercept for the Great Plains heat flow province. The heat generation measured at these sites is three times greater than the average for the area. It is possible that the samples measured at these sites are not representative of the upper crust. The reduced heat flow values of 0.89 and 0.85 HFU at San Pedro suggest that this area is part of the Great Plains heat flow province. Reduced heat flow values of 2.1 HFU at Crested Butte and >3.2 HFU in the Jemez Mountains suggest additional nonradioactive, thermal sources within the crust and upper mantle. The reduced heat flow value of 1.1 at Animas Peak is somewhat low for the Basin and Range. The value of 1.4 HFU at Orogrande is appropriate for the Basin and Range. The noise level of all reduced heat flow measurements in the area is quite high and caution should be exercised when considering the significance of the value at a single site.

APPENDIX I

TEMPERATURE AND THERMAL CONDUCTIVITY MEASUREMENTS

Measurement of the Geothermal Gradient

Temperature measurements in boreholes are typically made by lowering a thermistor probe to discrete depths and allowing the probe to come into thermal equilibrium with its surroundings. Normally measurements are made every ten meters except in boreholes greater than 1 km deep where time restrictions normally force one to use 20 meter increments. Temperature measurements are made as the cable is lowered into the drill test so that the cable disturbs the borehole very little before the temperature measurement is taken.

Two types of thermistor probes are used for borehole temperature measurements, a 1% 4K isocurve Fenwall probe and a 2% 4K isocurve Fenwall probe. Mueller-type resistance bridges are used to measure the resistance of the probes. The absolute accuracy of the borehole temperature measurements is ±0.05°C; the relative accuracy between two points ten meters apart is probably 0.005°C.

The thermistor probes are calibrated at 0.0°C in a circulating ice bath. They are also cross-checked with a platinum temperature sensing device at several other water temperatures in a circulating bath.

Measurement of the Thermal Conductivity

Thermal conductivities of rock core and rock fragment samples are measured both on an absolute apparatus (Reiter and Hartman, 1971) and on a divided-bar apparatus (Birch, 1950). Both techniques will be explained briefly. A schematic diagram of the divided bar apparatus is shown in figure 6. The fused quartz standards are GE 125 silica with a thermal conductivity of 3.28 (Ratcliff, 1959). Copper-constantan thermocouples were used to measure the temperature drop across each fused quartz standard and across the rock sample. A K-9 Leeds and Northrup potentiometer is used to measure the voltages across each thermocouple pair. By measuring the thickness and the temperature drop, the temperature gradients can be calculated for the quartz reference discs and the rock sample. By insulating the entire "stack" with polyurethane, radial heat losses are minimized. Assuming thermal equilibrium and no radial heat losses, the heat flux through the stack is constant and we can write

$$Q = \frac{K_F}{A_1}\frac{\Delta T_1}{\Delta Z_1} = \frac{K_R}{A_R}\frac{\Delta T_2}{\Delta Z_2} = \frac{K_F}{A_3}\frac{\Delta T_3}{\Delta Z_3}$$

or

$$K_R = \frac{K_F}{2}\left(\frac{\Delta T_1}{A_1 \Delta Z_1} + \frac{\Delta T_3}{A_3 \Delta Z_3}\right)\left(\frac{\Delta Z_2}{\Delta T_2}\right)A_R$$

where

K_R = thermal conductivity of the rock sample

K_F = thermal conductivity of the reference discs

ΔT_1 = temperature drop across the upper reference disc

Figure 6. Schematic drawing of the Divided Bar Thermal Conductivity Apparatus

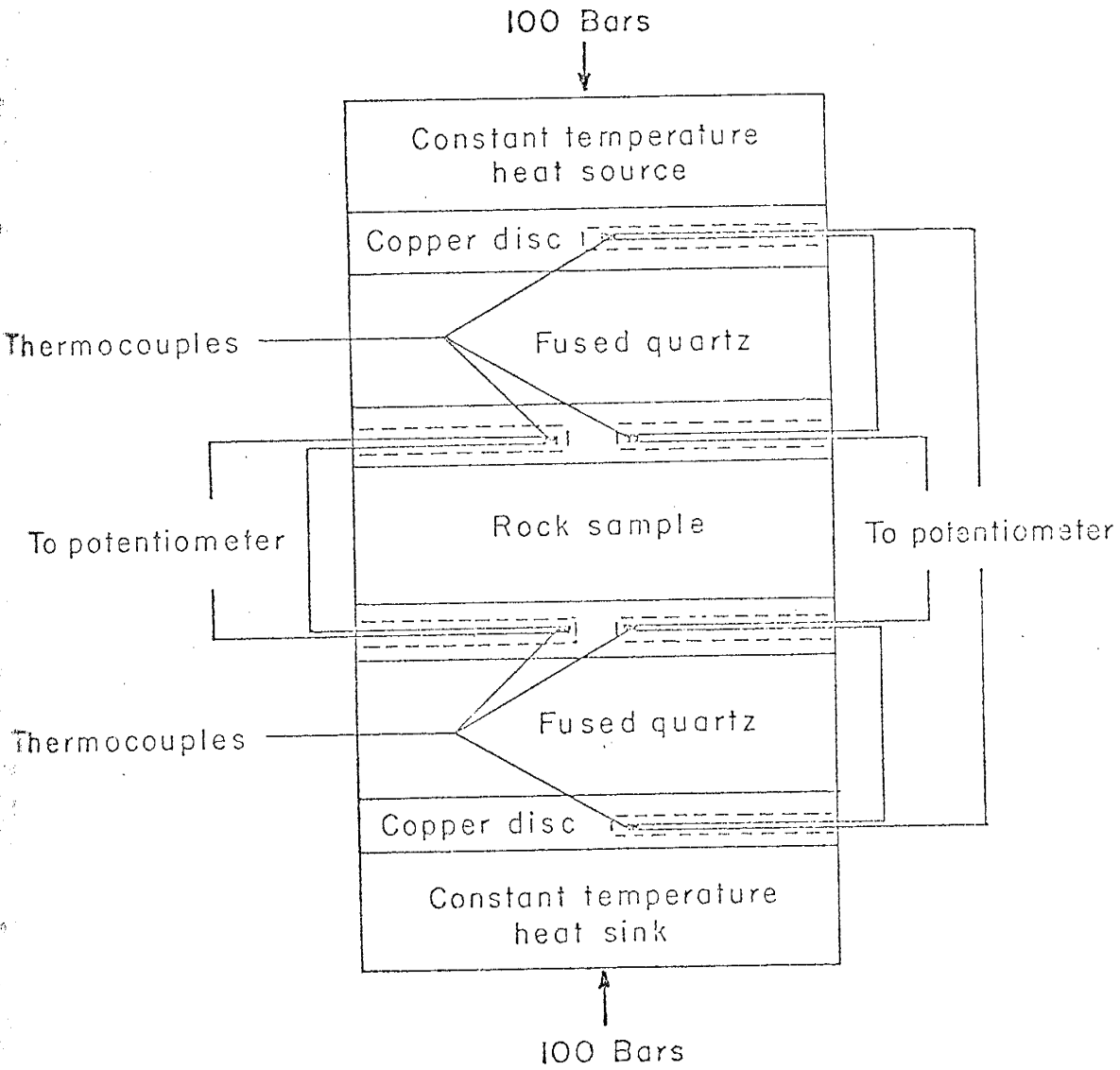

ΔZ_1 = thickness of the upper reference disc

A_1 = cross-sectional area of the upper reference disc

ΔT_2 = temperature drop across the rock sample

ΔZ_2 = thickness of the rock sample

A_2 = cross-sectional area of the rock sample

ΔT_3 = temperature drop across the lower reference disc

ΔZ_3 = thickness of the lower reference disc

A_3 = cross-sectional area of the lower reference disc

A schematic diagram of the absolute thermal conductivity apparatus is given in figure 7. The constant flux source is a precision resistor mounted on a copper disc. By using a precision constant voltage power supply and measuring the voltage and current to the resistor, the power generated by resistor can be calculated. The heat sink is a massive aluminum block. By insulating the entire stack and the heater with polyurethene, we can minimize the radial heat loss. Assuming thermal equilibrium and no radial heat losses, the heat flux through the stack is

$$Q = VI = \frac{K_R \Delta T_1}{A_R \Delta Z_1}$$

or

$$K_R = \frac{VI\ A_R\ \Delta Z_1}{\Delta T_1}$$

where

K_R = thermal conductivity of the rock sample

V = voltage across the heater

I = current through the heater

A_R = area of the rock sample

Figure 7. Schematic drawing of the 'Absolute' thermal Corductivity Apparatus

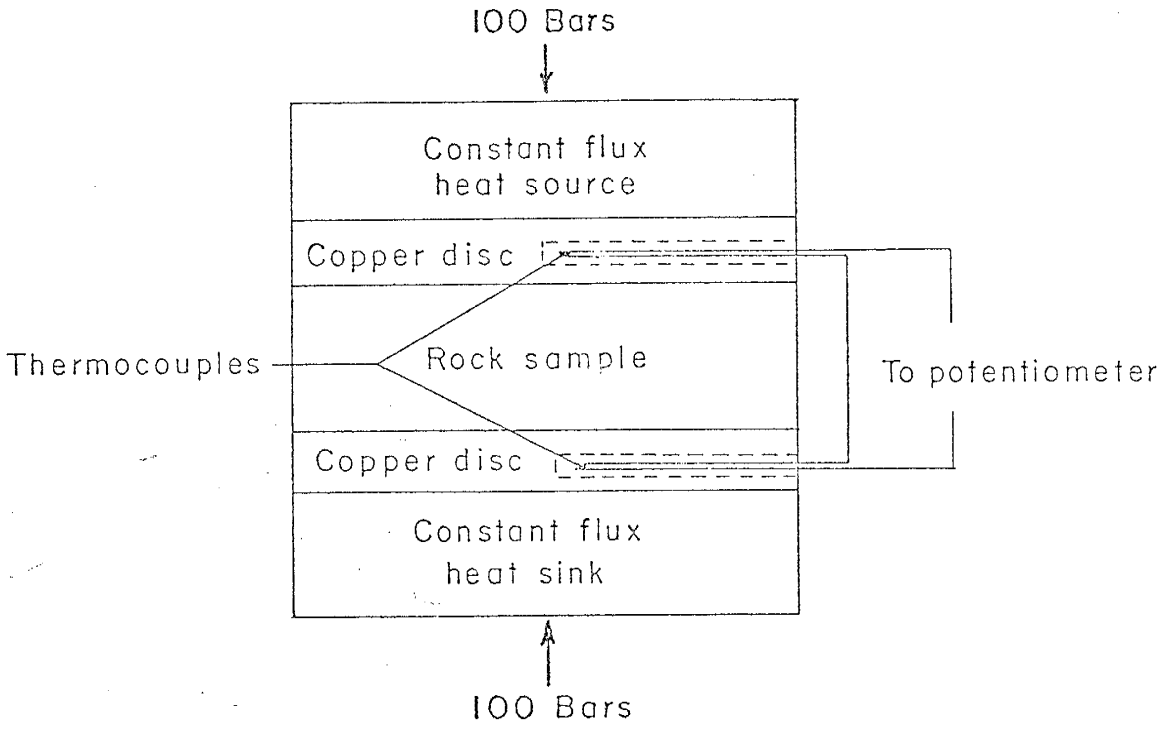

ΔZ_1 = thickness of the rock sample

ΔT_1 = temperature drop across the rock sample

Thermal conductivity of both core and fragment samples is measured. The core samples consist of wafers from 1 to 2 centimeters long whose surfaces were lapped flat and parallel within ±.005 cm.

The thermal conductivity of fragment samples is measured using a technique like that of Sass and others (1971 b). Cylindrical cells the approximate size of the large core samples are constructed with copper faces and plastic sides and then filled with water saturated rock fragments. The cell is then measured as if it were a core sample. The thermal conductivity of the fragments is given by

$$K_{pr} = K_w \left[\left(\frac{D^2}{d^2} \right) \left(\frac{K_c}{K_w} \right) - \left(\frac{D^2 - d^2}{d^2} \right) \left(\frac{K_p}{K_w} \right) \right] \left(\frac{1-\phi_o}{1-\phi} \right)$$

where

D = outer diameter of the cell wall

d = inner diameter of the cell wall

K_p = thermal conductivity of the plastic of cell wall

K_w = thermal conductivity of water

K_c = measured thermal conductivity of the cell and its contents

K_{pr} = conductivity of the porous rock

ϕ_o = natural porosity of the rock sample

ϕ = volume fraction of the water in the cell

Core samples are measured saturated or dry, depending on the sample depth and the depth to the water table.

Samples are saturated by placing the sample in a vacuum chamber, evacuating the air, and then flooding the chamber with distilled water.

All fragment samples are vacuum flooded since at present there is not a technique available for measuring dry fragment samples.

The thermal conductivity apparatus is regularly calibrated with wafers of fused and crystalline quartz. Fused quartz and several other secondary standards in fragment form are used to insure the reliability of the rock fragment measurements.

Corrections to the Thermal Conductivity

The three principle corrections to the thermal conductivity measurements are for the effects due to temperature, to pressure, and to the presence of interstitial fluids. Temperature coefficients for dolomite are approximately 2%/10°C (Handbook of Physical Constants). The mean temperature of all the wells logged is about 18°C with an average range of 14-22°C. In most cases the sample is measured at 20°C. The error due to temperature is then less than 1% in most cases.

The pressure effect on conductivity in the range of 100-200 bars on low porosity rocks is about 2% to 3% (Walsh and Decker, 1966). Core samples in this study are measured under an axial pressure of on the order of 100 bars. Fragment samples are measured under an axial load of one bar.

The effects of interstitial fluids in samples are compensated by vacuum flooding which fills the connected pore spaces with fluid. Those core samples which appear to be above the water table are measured dry.

We believe the net correction for temperature and pressure to be less than 5%. Since the reproducibility of thermal conductivity measurements is 5-10% for core and 10-15% for fragments, no correction for temperature or pressure is made.

APPENDIX II

ERRORS IN HEAT FLOW VALUES

Regional ground water movement and channel water movement in the borehole are the primary causes of nonrepresentative heat flow measurements. In some cases the disturbed zones can be identified and removed from the analysis (Reiter and others, 1975). The Nolan/East well (figure 8) shows three temperature gradient zones, 35°C/km between 40-80 m, 43°C/km between 80-140 m, and 55°C/km between 140-180 m. There are no thermal conductivity samples available for the top zone. The middle and bottom zones give heat fluxes of 2.7 and 2.8 HFU respectively. There is no additional information available which would indicate that deeper regional ground water movement is altering the heat flux. The heat flux 2.75 HFU, the mean of the two zones, is thought to be representative of the area.

The Sierra del Ohito well (figure 9) probably shows the effect of horizontal ground water flow in the upper 200 m of the hole. Since the hole was cased and water was not flowing at the surface, vertical water movement in the casing is precluded. The temperature depth plot in the upper 200 m of the test can result from horizontal groundwater movement in the aquifer (McFadden, personal communication) or from vertical groundwater movement in the anulus between the casing and the hole.

Even though there is a near zero temperature gradient in the top of the hole, the middle gradient (64°C/km between 250-350 m) and the bottom gradient (58°C/km between 350-470 m) give heat fluxes of 2.6 and 2.4 HFU respectively. The mean heat flow (2.5 HFU) for the well appears in reasonable agreement with other sites in the area.

The Turkey Creek borehole (figure 10) shows how the vertical component of ground water movement may affect the temperature gradient in a zone of constant thermal conductivity. This borehole penetrates a shale which confines an artesian aquifer. The concave down shape of the temperature-depth curve indicates a vertical component of water flow upward through the confining shale (Bredehoft and Papadopules, 1965). As the water moves upward it gives up part of its heat to its surroundings, increasing the rock temperatures until the water comes into thermal equilibrium with the rock. It is usually impossible to calculate the heat flux because so few of the hydrologic parameters can be specified.

The Tesuque well (figure 11) was cased with perforated well casing over the entire depth of the hole. Water movement within the borehole is believed to cause the eratic temperatures. When the temperature gradients are correlated with the respective thermal conductivities, the heat fluxes are not constant.

The Golden well (figure 12) has two linear gradient zones, 27°C/km between 80-150 m and 19°C/km between 150-250 m. However, the heat fluxes are significantly different, 2.6 HFU in the top zone and 1.2 HFU in the bottom zone. The

heat flow in the bottom zone (1.2 HFU) is consistant with other data points in the area. Ground water movement appears to be fracture controlled in much of the area and is possibly causing the discrepancy between the heat flow of the two zones. Ground water moving along fracture zones can increase or decrease the undisturbed temperature of the fractured rock. If the flow continues, the natural geothermal gradient above and below the fracture zone will change to accommodate this new boundary condition and the resultant heat flows may be higher or lower than the natural undisturbed heat flow depending on the temperature of the water flowing through the fracture zone. The Ortiz #3 borehole (figure 13) probably shows this effect too. Ground water at a temperature less than that predicted by the natural geothermal gradient is flowing through a fracture zone at a depth of 300 m. This cooler water lowers the gradient above the fracture zone and increases the gradient below the fracture zone. The heat flow is 1.2 HFU in the upper zone and 1.4 HFU in the lower zone. The average heat flow for the area is about 1.3 HFU.

The Ortiz #2 borehole (figure 14) exhibits a long linear gradient, 18°C/km between 140-170 m, which correlates with the thermal conductivity values to give a heat flux of 1.3 HFU. Although some other boreholes in the area (Ortiz #1, Ortiz #3, Ortiz #4, and Golden) exhibit some influence of water movement, there does not appear to be any such disturbances in this temperature log.

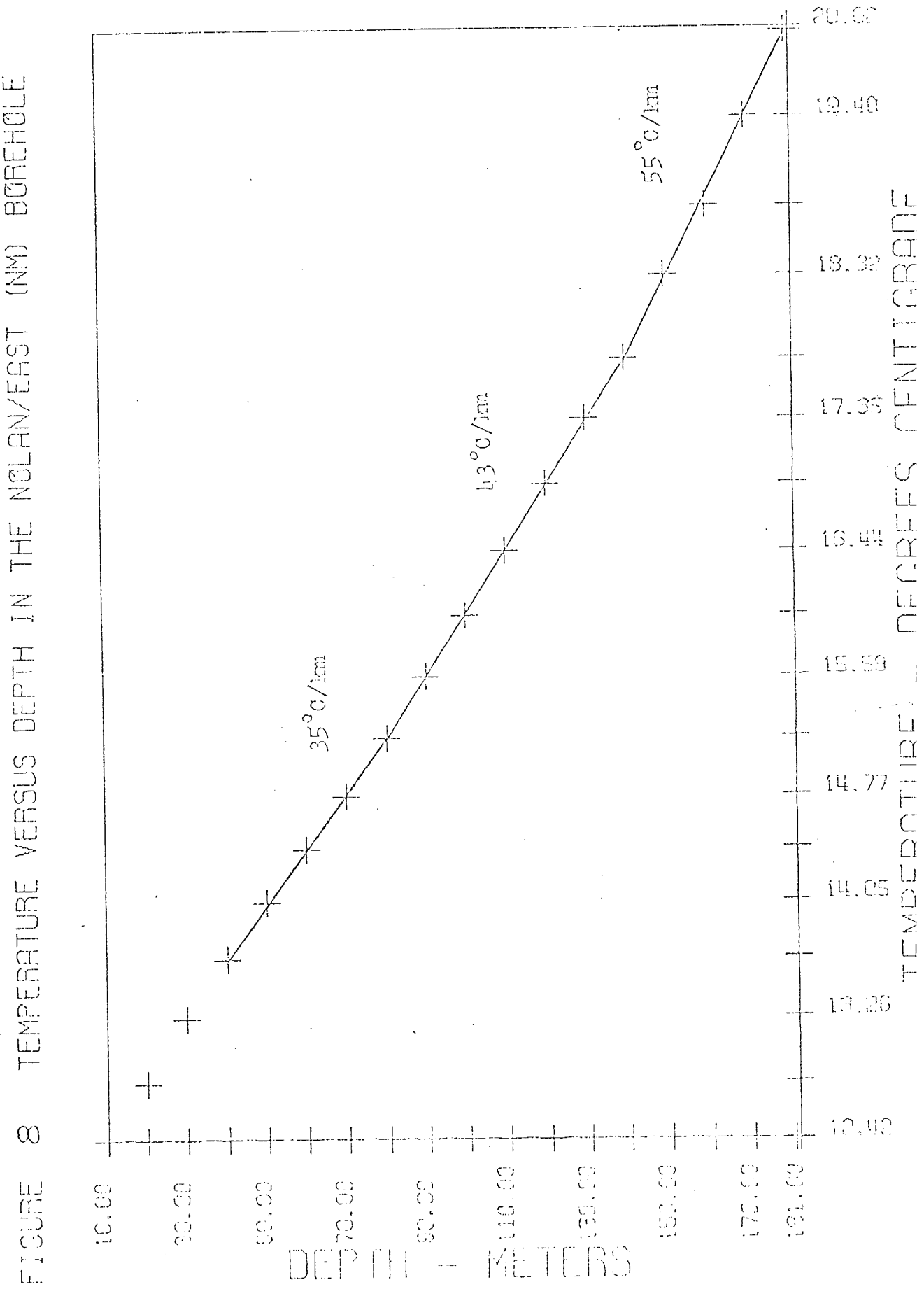
FIGURE 8 TEMPERATURE VERSUS DEPTH IN THE NOLAN/EAST (NM) BOREHOLE
DEPTH - METERS
TEMPERATURE - DEGREES CENTIGRADE
35°c/km
43°c/km
55°c/km
10.00
30.00
50.00
70.00
90.00
110.00
130.00
150.00
170.00
191.00
20.00
19.40
18.80
17.36
16.44
15.59
14.77
14.05
13.26
12.43

FIGURE 9 TEMPERATURE VERSUS DEPTH IN THE SIERRA DEL CUITO (C) BARREALE

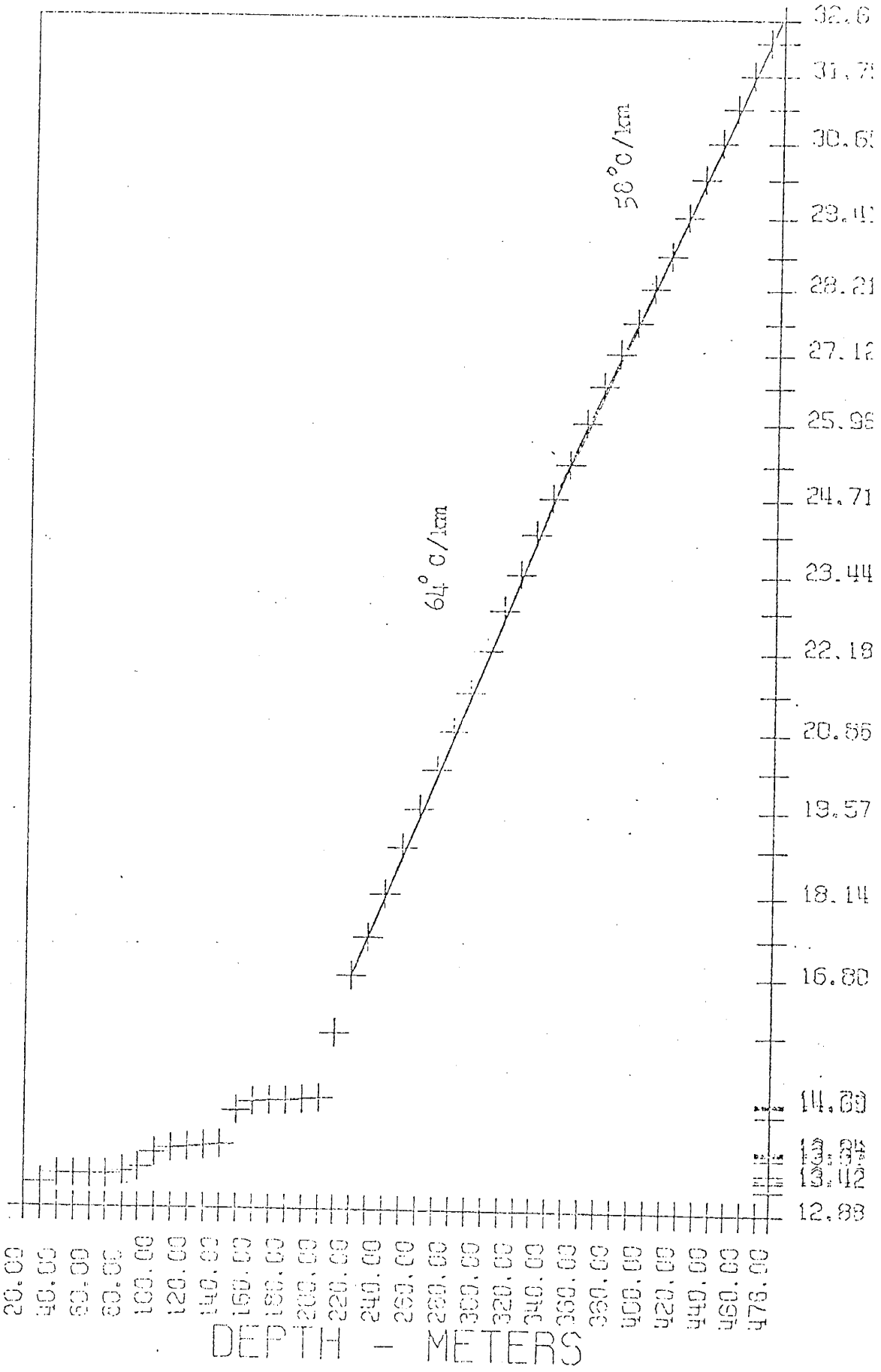

FIGURE 10 TEMPERATURE VERSUS DEPTH IN THE TURKEY CREEK BOREHOLE

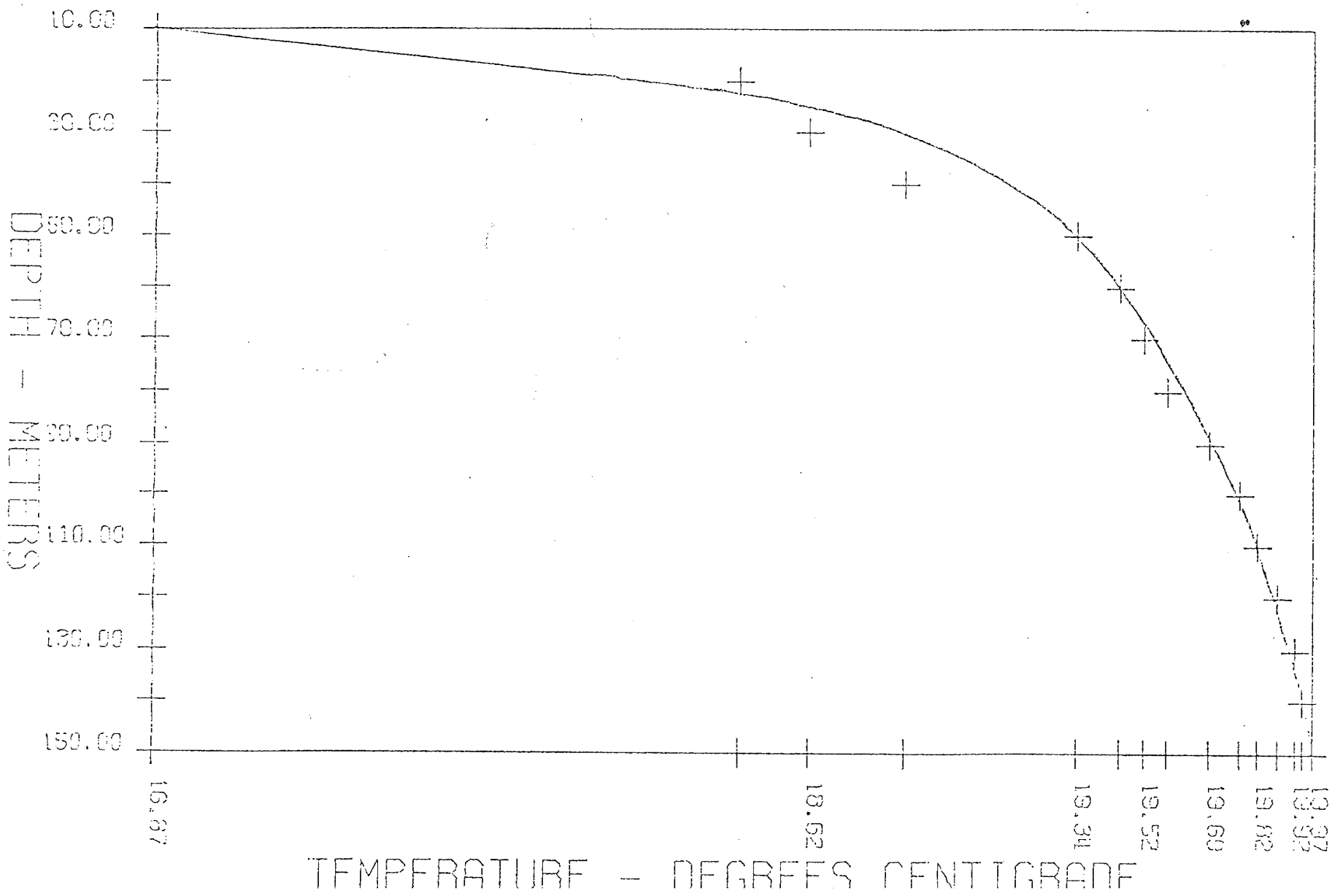

FIGURE 11 TEMPERATURE VERSUS DEPTH IN THE TESUQUE (NM) BOREHOLE

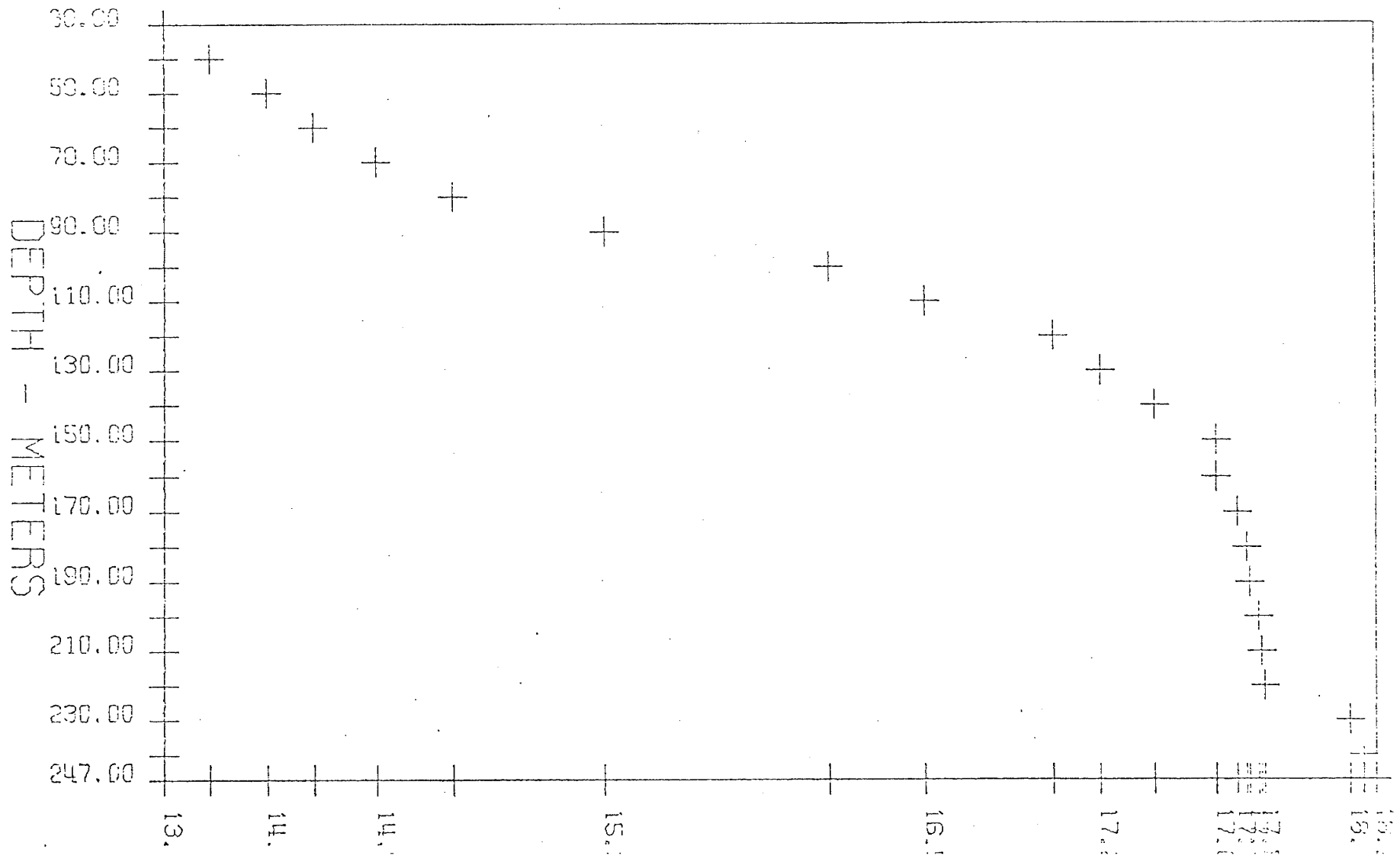

FIGURE 12 TEMPERATURE VERSUS DEPTH IN THE GOLDEN #1 BOREHOLE

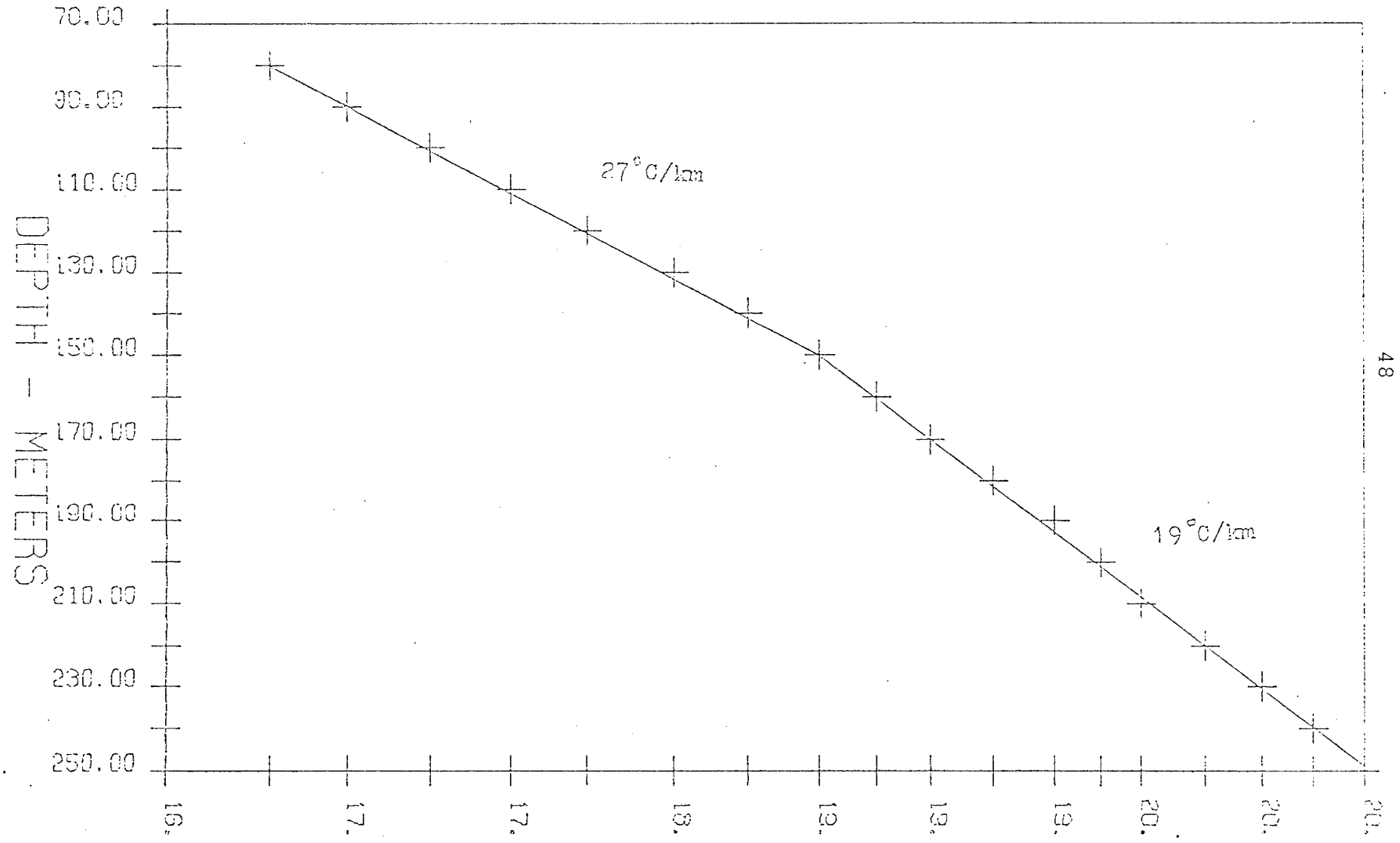

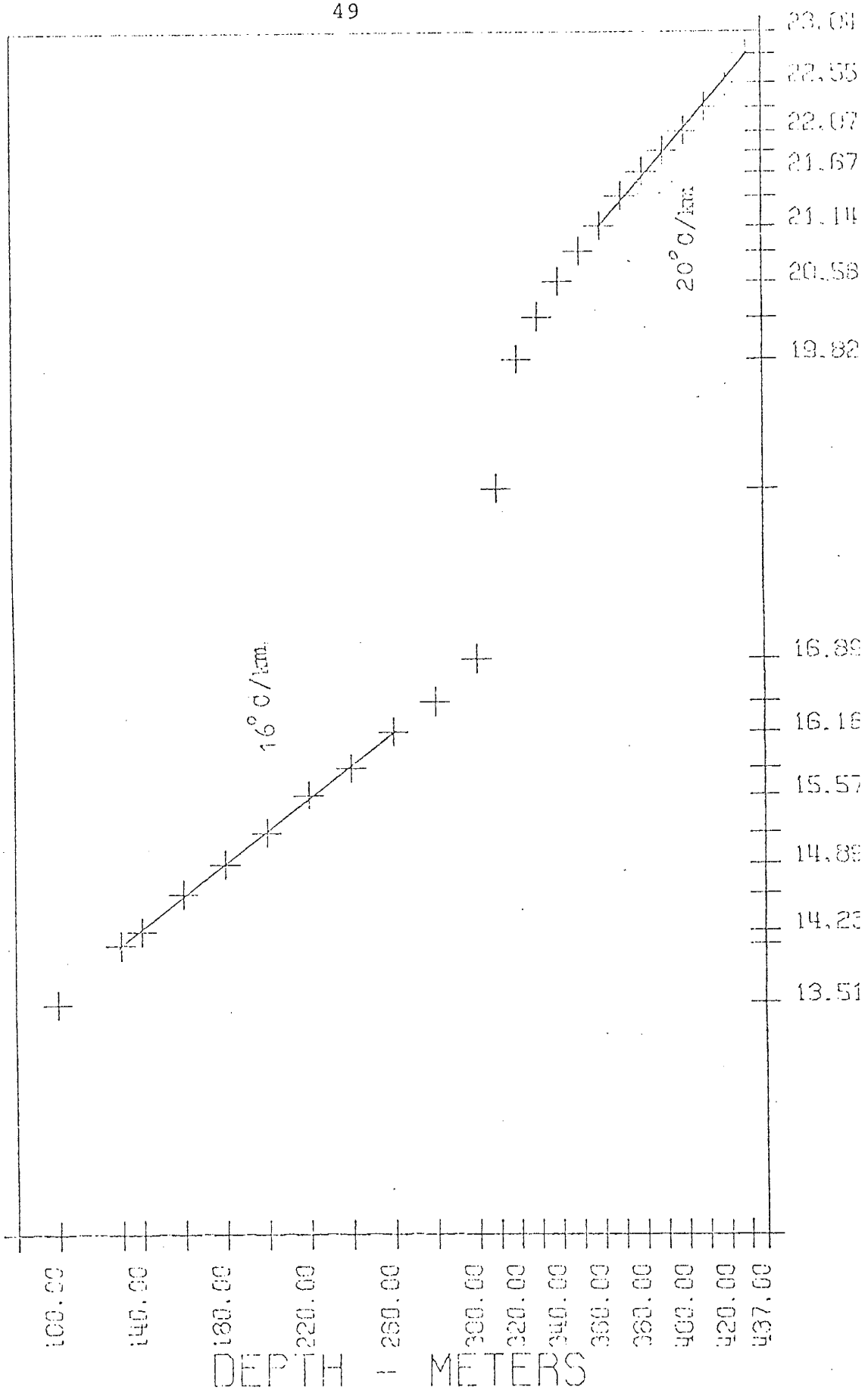

FIGURE 13 TEMPERATURE VERSUS DEPTH IN THE ORTIZ #3 BOREHOLE

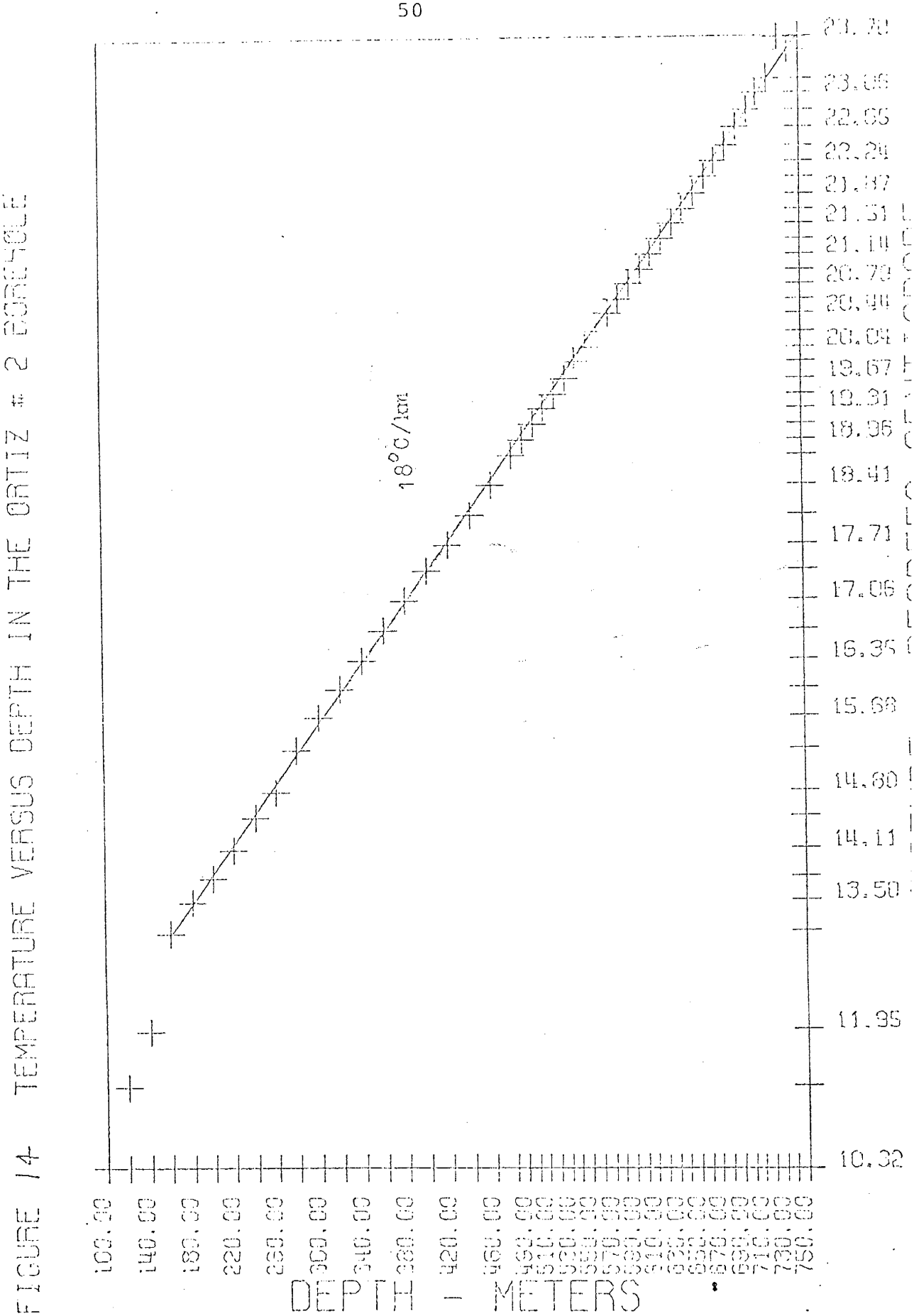

FIGURE 14 TEMPERATURE VERSUS DEPTH IN THE ORTIZ # 2 BOREHOLE

APPENDIX III

MEASUREMENT OF POTASSIUM, URANIUM AND THORIUM CONCENTRATIONS AND DETERMINATION OF THE HEAT PRODUCTION

Computational Scheme

Three naturally occurring radioactive elements, uranium, thorium and potassium, with their daughter isotopes, generate over 99% of the heat due to radioactive decay in rocks (Stacey, 1969). The gamma ray spectra of the rock samples used in this study are measured by a Nuclear Data 512 channel analyzer system with a sodium iodide detector of 7.5 cm diameter and 7.5 cm length. The spectra are interpreted with the aid of a linear least squares computer technique which matches the sample spectrum to a library spectrum generated by the superposition of uranium, thorium and potassium spectra. The measured gamma ray spectra of potassium, uranium, thorium and a rock sample are shown in figures 15-18.

The technique used to calculate the radioelement concentrations is described by Rybach (1971) and is briefly described here. Figure 15 shows the measured gamma-ray spectrum of a typical rock sample. The superposition of the potassium, uranium and thorium spectra (figures 16, 17, and 18) can give the observed rock spectrum if they are weighted as in the following expression

$$d_i = a_i M_K + b_i M_U + c_i M_{Th} \qquad \text{(equation 1)}$$

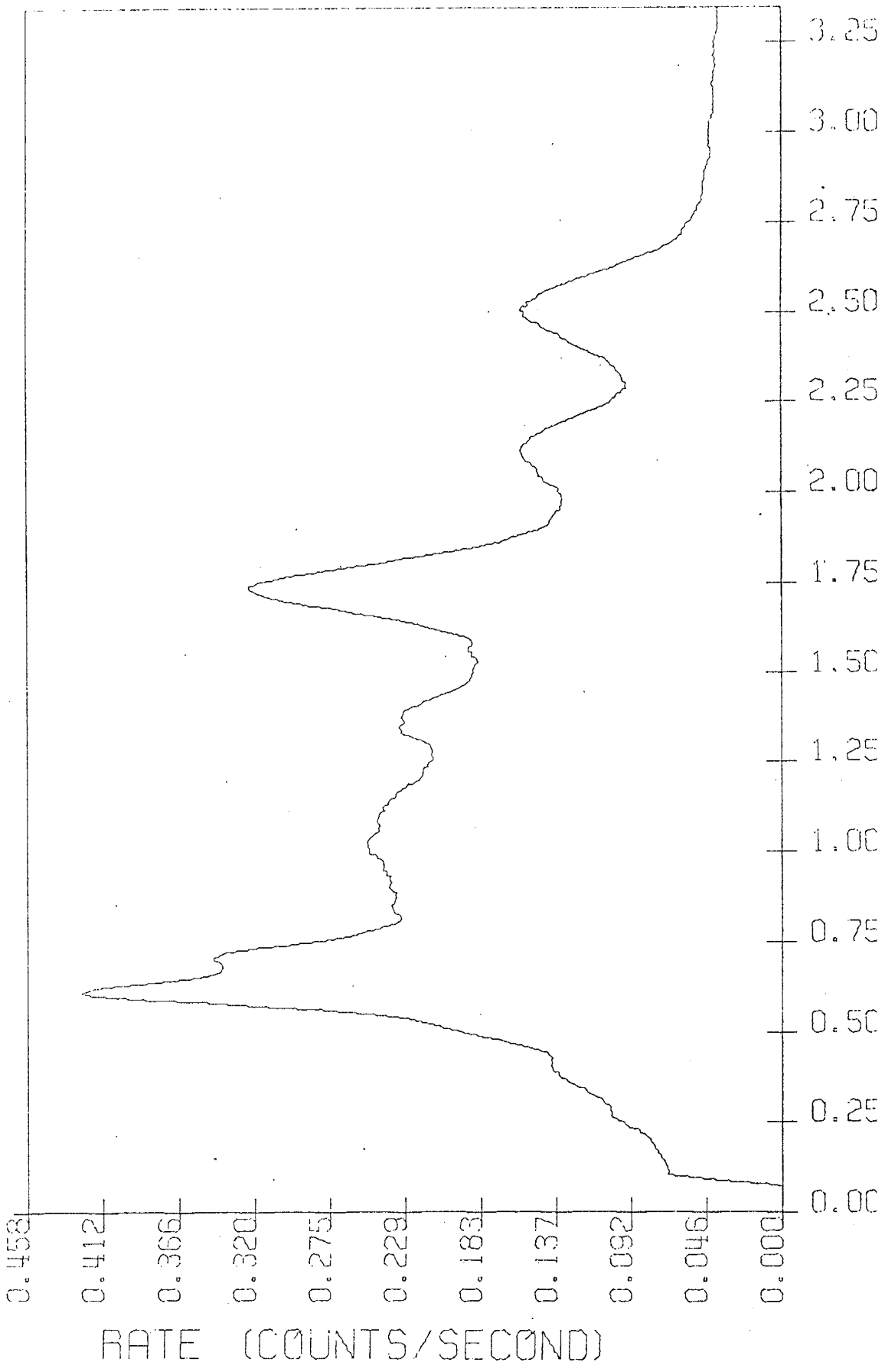

Figure 15 Gamma Ray Spectrum of a Rock Sample

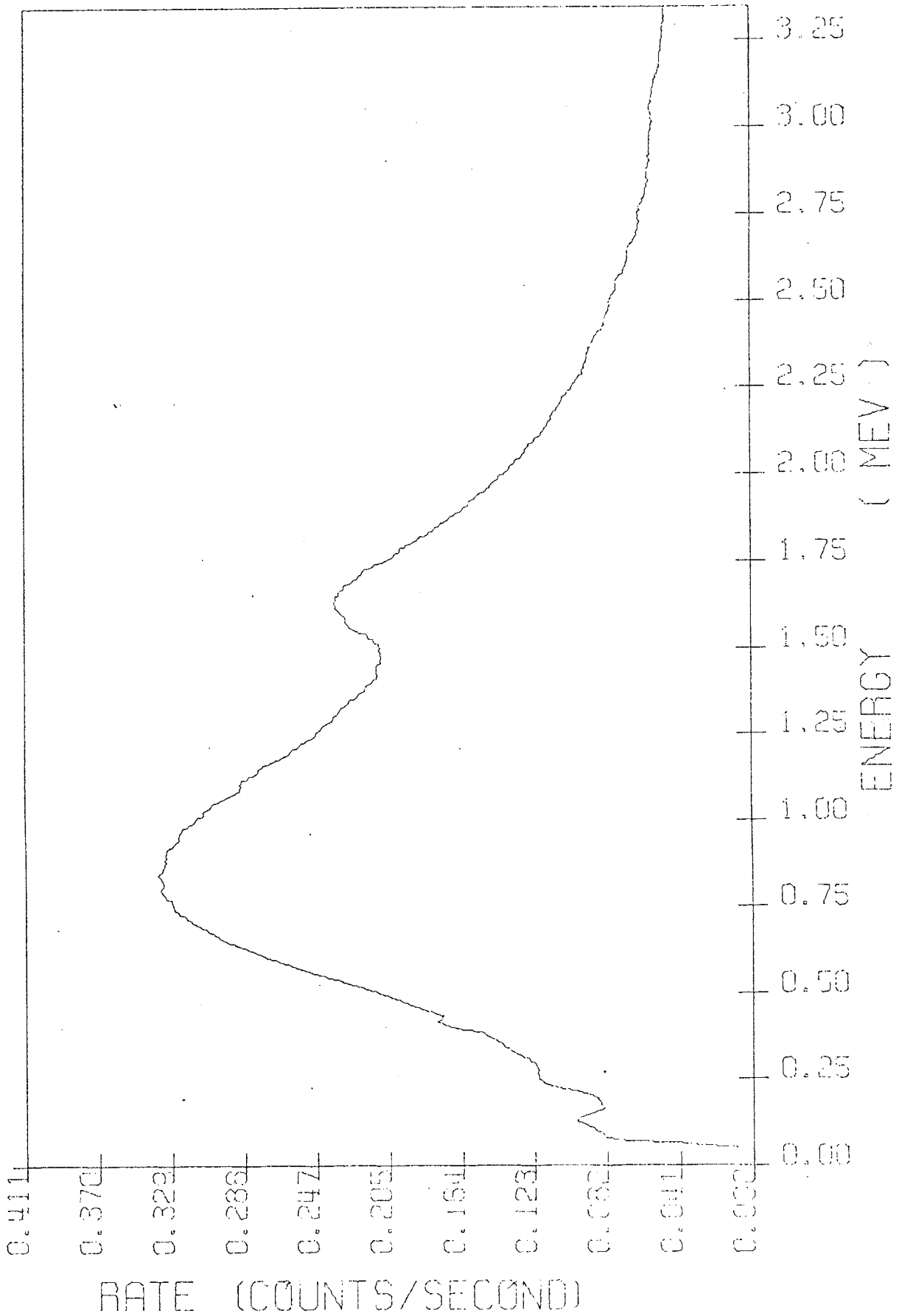

Figure 16 Gamma Ray Spectrum of Potassium

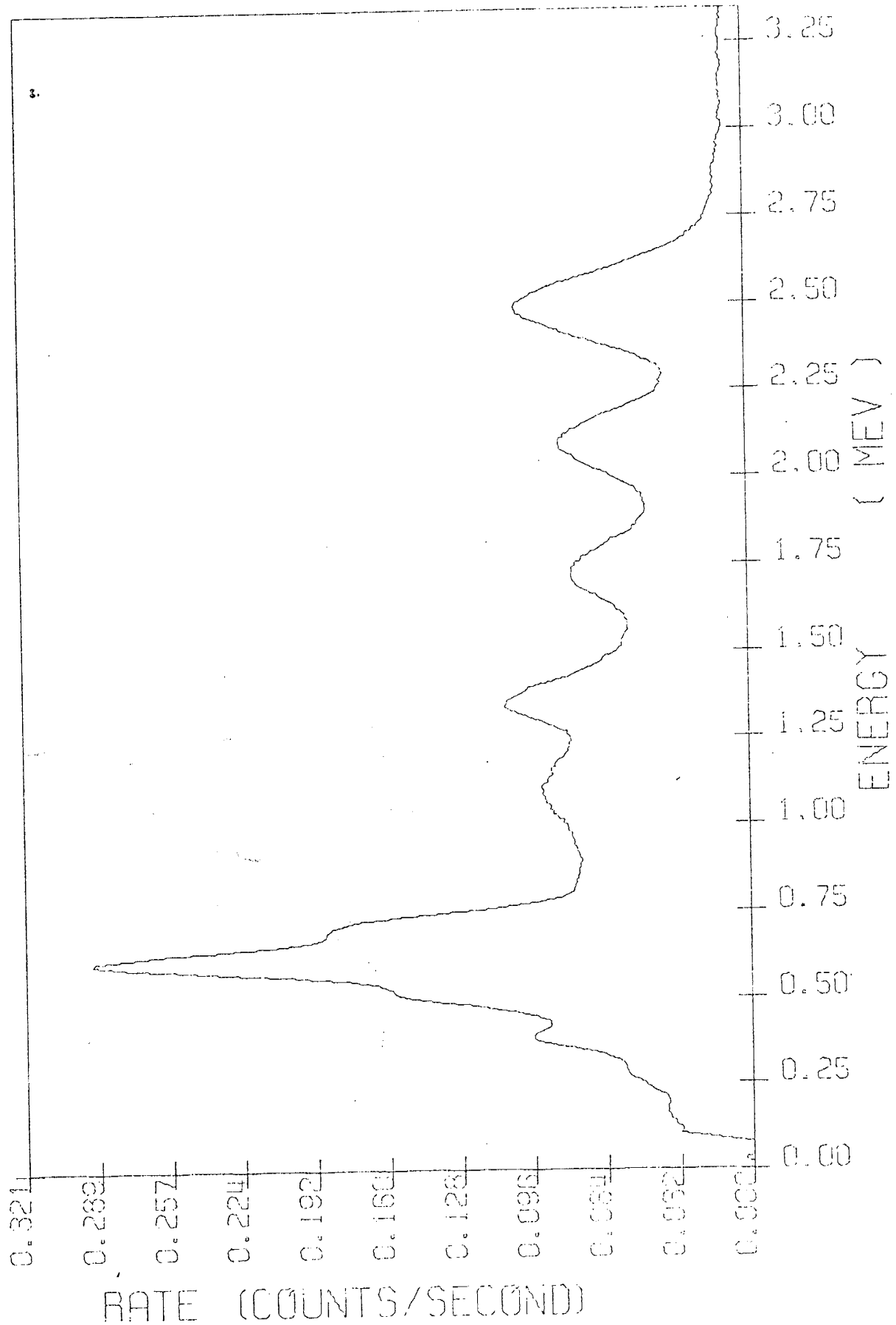

Figure 17 Gamma Ray Spectrum of Uranium

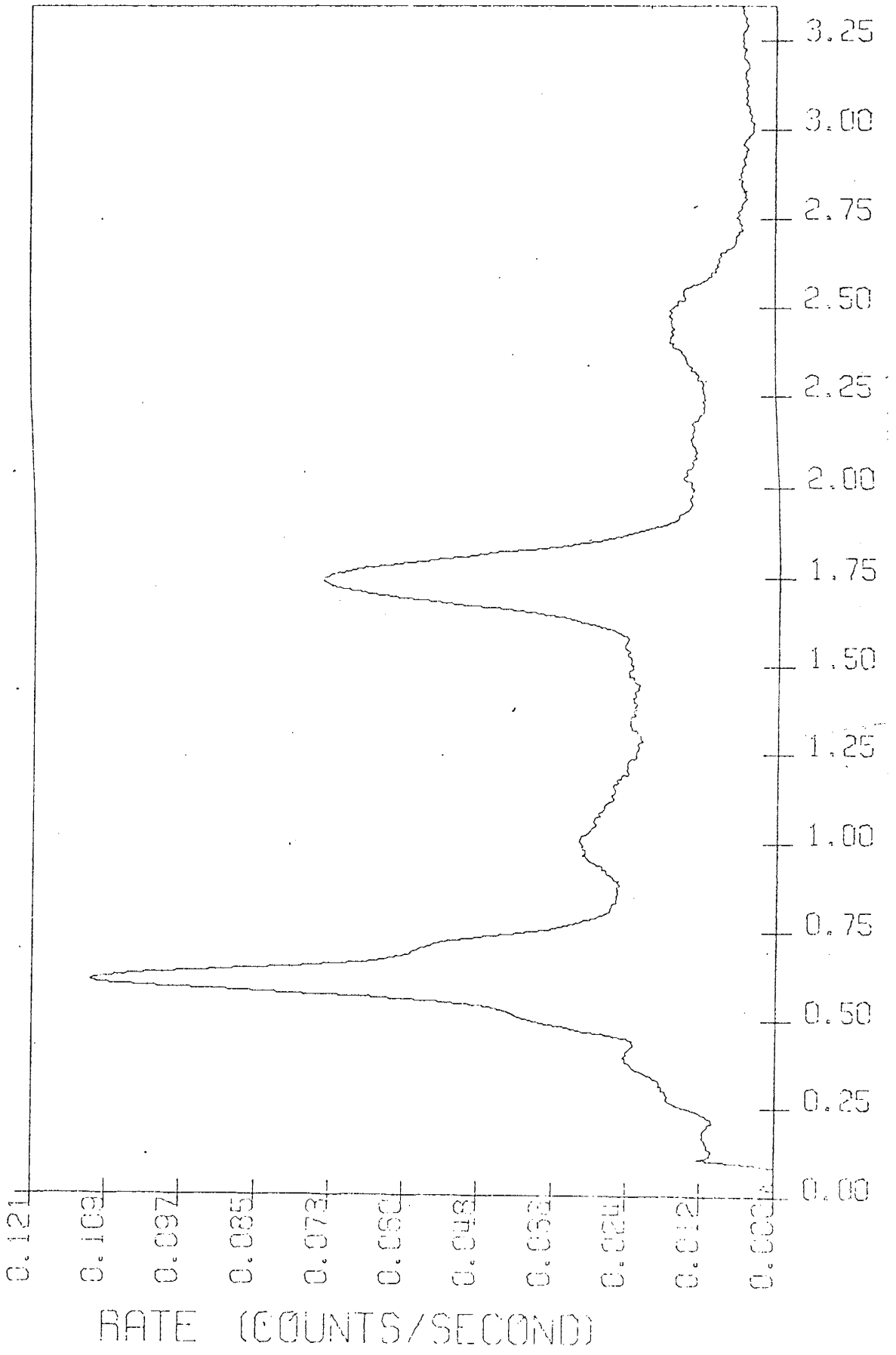

Figure 18 Gamma Ray Spectrum of Thorium

where

i = channel number, $i = 1, 2, \ldots 511$

d_i = counting rate in the ith channel (counts per second)

M_K = mass of potassium in the sample (grams)

M_U = mass of uranium in the sample (grams)

M_{Th} = mass of thorium in the sample (grams)

a_i, b_i, c_i = undetermined constants of proportionality

To determine a_i, b_i, c_i, three standards are used, a potassium standard, a uranium standard and a thorium standard. The potassium standard used is potassium bromide. The uranium standard is NBL-77-A obtained from the New Brunswick Laboratory (concentration of uranium = 10 ppm). The thorium standard is NBL-86-A also obtained from the New Brunswick Laboratory (concentration of thorium = 10 ppm).

For the potassium standard alone equation 1 becomes

$$d_i = d_i' = a_i M_K \qquad \text{(equation 2)}$$

For the uranium standard alone equation 1 becomes:

$$d_i = d_i'' = b_i M_U \qquad \text{(equation 3)}$$

For the thorium standard alone equation 1 becomes:

$$d_i = d_i''' = c_i M_{Th} \qquad \text{(equation 4)}$$

When a_i, b_i and c_i are found by measuring the spectra of potassium, uranium and thorium separately, the concentrations of potassium, uranium and thorium in any rock sample may be estimated by measuring d_i and

solving the following matrix equation

$$\begin{pmatrix} d_1 \\ d_2 \\ d_3 \\ . \\ . \\ d_{511} \end{pmatrix} = \begin{pmatrix} a_1 & b_1 & c_1 \\ a_2 & b_2 & c_2 \\ a_3 & b_3 & c_3 \\ . & . & . \\ . & . & . \\ a_{511} & b_{511} & c_{511} \end{pmatrix} \begin{pmatrix} M_K \\ M_U \\ M_{Th} \end{pmatrix} \qquad \text{(equation 5)}$$

Having 511 equations and only three unknowns, M_K, M_U, and M_{Th}, a least-squares technique is used to determine the "best values" of M_K, M_U, and M_{Th} as follows

$$\sum_{i=1}^{511} \left[d_i - (a_i M_K + b_i M_U + c_i M_{Th}) \right]^2 = S \qquad \text{(equation 6)}$$

M_K, M_U, and M_{Th} are determined so that S is a minimum (Hays and Winkler, 1971). The unknown masses M_K, M_U, and M_{Th} for each sample are calculated on an IBM 360-44 computer using the least-squares technique. The computer programs and subroutines are summarized in Appendix III.

Calibration of the System

To check the absolute accuracy of the system, five samples with known concentrations of uranium, potassium and thorium are measured. The concentrations of these samples are listed in Table 5. The measured values of M_K, M_U and M_{Th} for the rock standards are systematically lower than the actual values. The actual masses are plotted against the measured masses of potassium, uranium and thorium, and

Table 5. Concentrations of Potassium, Uranium and Thorium in the Standards.

Name	Potassium (%)	Uranium (ppm)	Thorium (ppm)
Standard #1*	3.5	1.5	3.5
Standard #5+	3.08	1.86	8.53
Standard #3+	6.75	3.64	6.75
Standard #2+	10.0	5.64	10.0
Standard #4+	15.0	9.83	15.0

*USGS Rock Standard G10-γ

+Samples mixed from potassium bromide, crystalline quartz, uranium and thorium samples supplied by the New Brunswick Laboratory.

a least-mean squares fit of a straight line through the data is used to correct for the systematic error. Figures 20, 21, 22 show the final results. The measured values of potassium, uranium and thorium differ by less than 10% from the actual values over the range of concentrations measured.

Sources of Error

Two experimental problems must be resolved before data measured with the gamma ray spectrometer can be used. The first problem is caused by the design of the electronics and is within the measured counting rate of the spectrometer. The spectrometer is unable to count every gamma ray that reaches the detector. As the count rate increases, the number of lost events increases because the counter is locked for a greater percentage of time processing data. To determine the actual counting rate from the measured counting rate, some correction must be applied to the measured counting rate. By counting thorium nitrate samples whose masses ranged from 0.001 g to 10.0 g we can plot mass versus total measured counting rate (figure 19).

As the mass is doubled the counting rate should also double. However, this is not observed. As shown graphically in figure 19, the total measured counting rate (R_M) is empirically related to the mass (M) of radioactive material as

$$\log M = 0.30 + 1.041 \log R_M \qquad \text{(equation 7)}$$

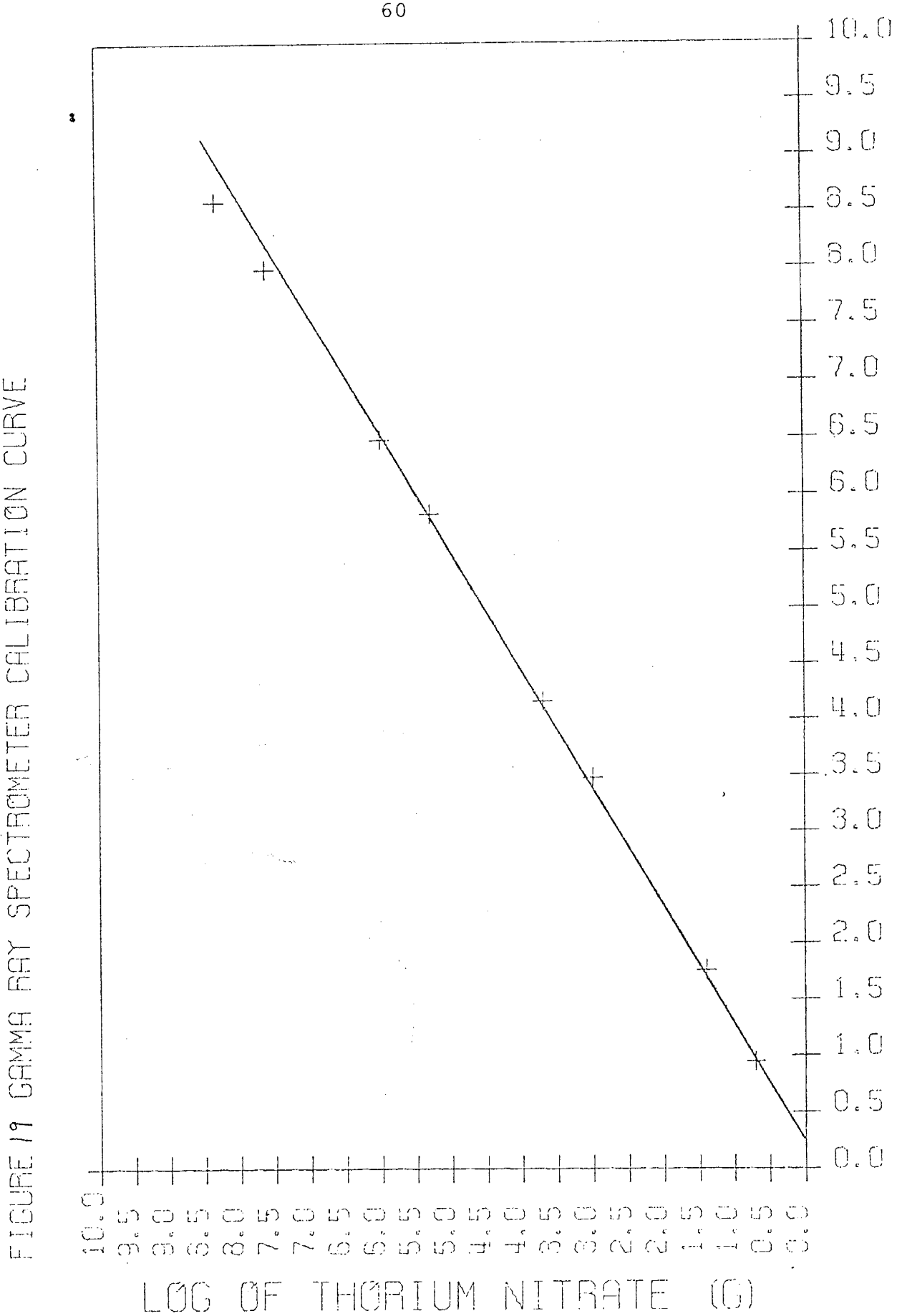

FIGURE 19 GAMMA RAY SPECTROMETER CALIBRATION CURVE

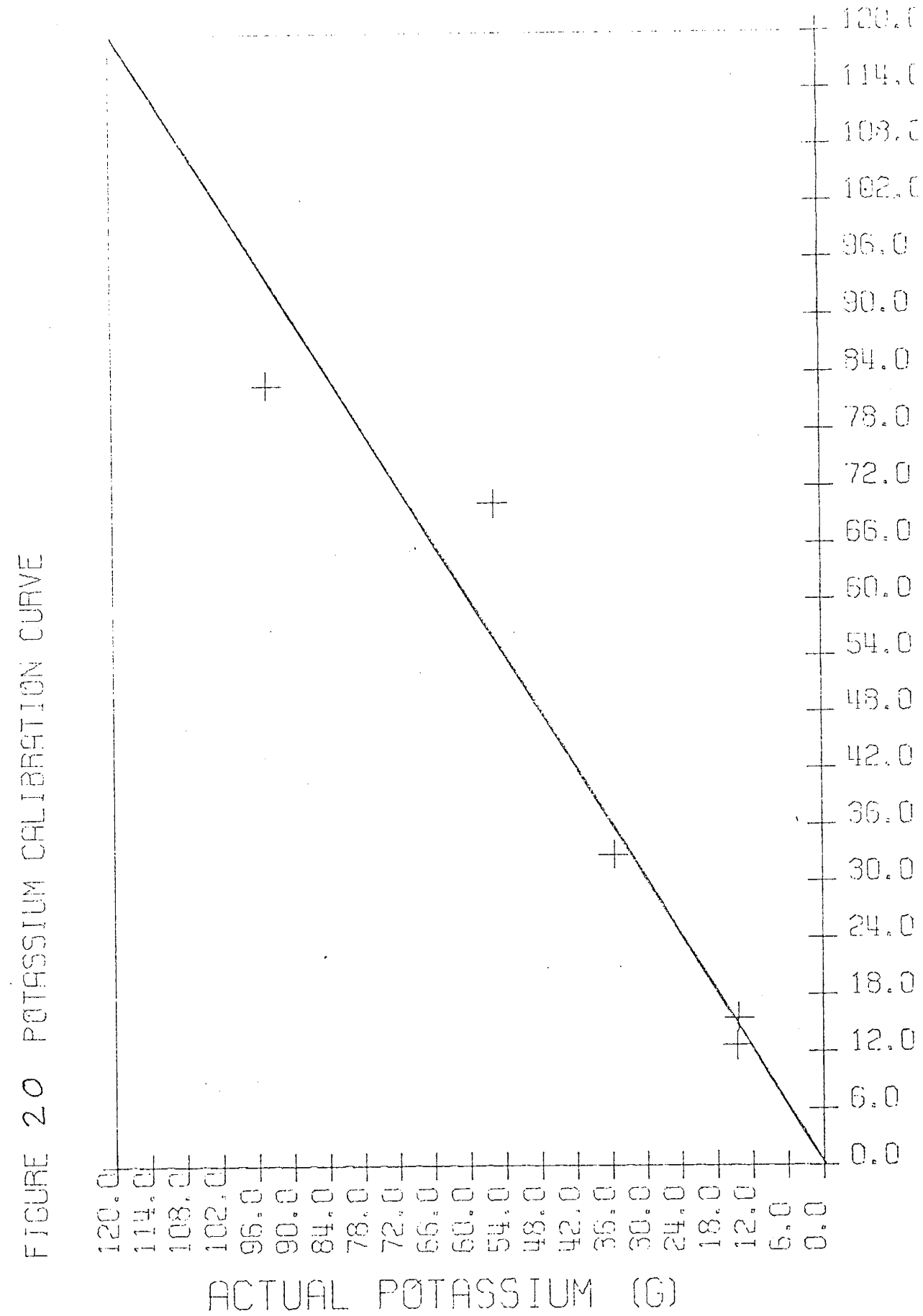

FIGURE 20 POTASSIUM CALIBRATION CURVE

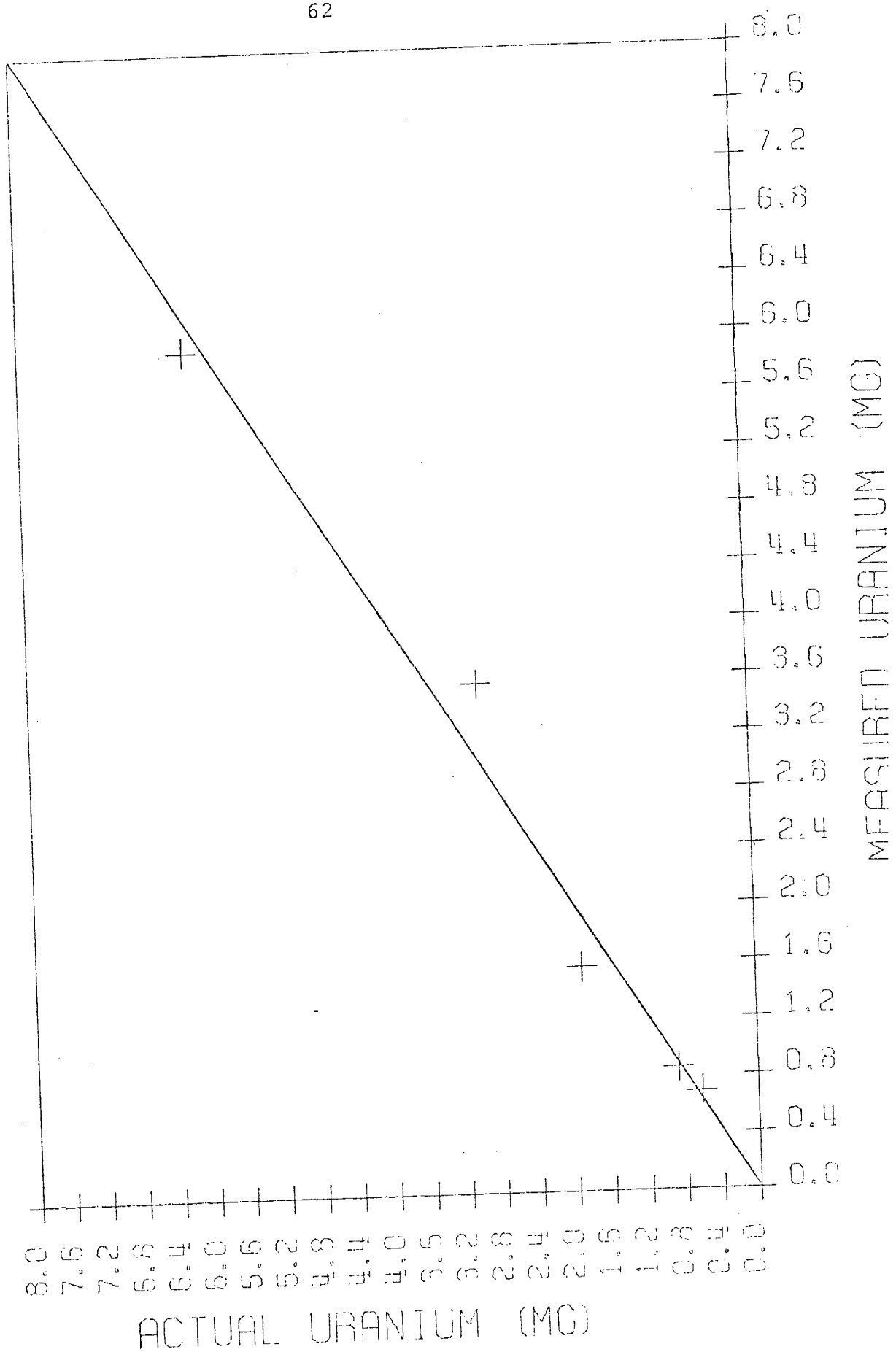

FIGURE 21 URANIUM CALIBRATION CURVE

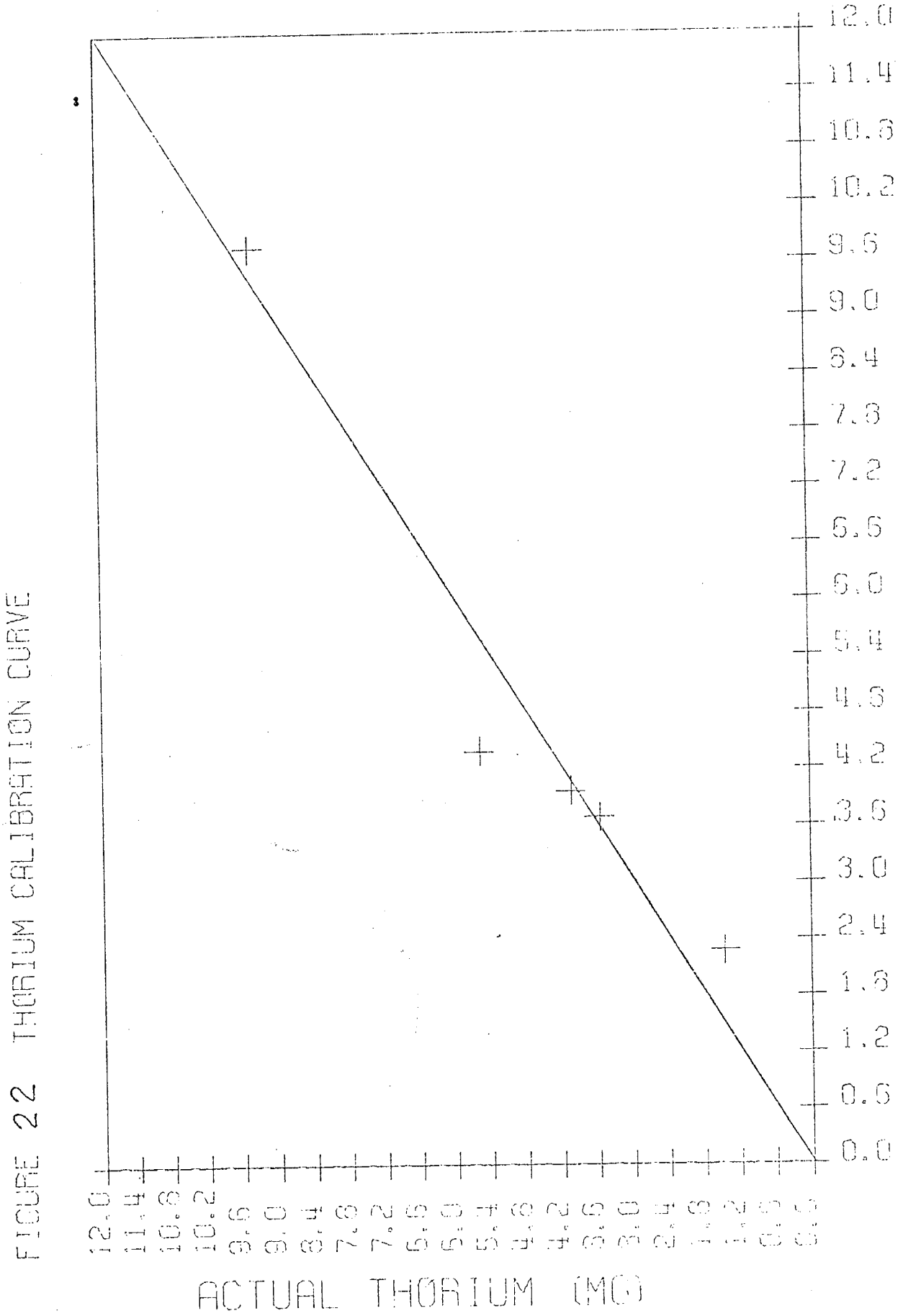

FIGURE 22 THORIUM CALIBRATION CURVE

The actual total counting rate (R_A) is then

$$\log R_A = 1.041 \log R_M \qquad \text{(equation 8)}$$

or

$$R_A = R_M^{1.041}$$

Using this empirical formula, the total number of counts lost over the spectrum per unit time can be determined. However, counts are not lost evenly across the spectrum. More counts are lost in the peaks than elsewhere in the spectrum because there is a higher probability of count loss in the peaks.

The corrected counting rate R_c in the i^{th} channel is given by Parzen (1962)

$$R_{ci} = \frac{R_{mi}}{1-L\,R_{mi}} \qquad \text{(equation 10)}$$

where R_{mi} is the measured counting rate in the i^{th} channel and L is the effective deadtime of the spectrometer. In a peak the value of R_{mi} is high, and therefore the quantity $(1-L\,R_{mi})$ decreases making the value of R_{ci} increase. In some samples measured, R_{ci} in the more prominent peaks is over 50% greater than R_{mi}. Away from the peaks in the gamma ray spectrum R_{mi} is small and the quantity $(1-L\,R_{mi})$ is almost equal to 1.0, consequently $R_{ci} \simeq R_{mi}$. The value of L is computed so that the increase in counting rate summed over 511 channels is equal to the difference between the actual total counting rate (R_A) and the measured total counting rate (R_M), that is:

$$\sum_{i=1}^{511} \left(R_{ci} - R_{mi}\right) = \left(R_A - R_M\right) \qquad \text{(equation 11)}$$

or $$\sum_{i=1}^{511} \left(\frac{R_{mi}}{1-L\ R_{mi}} - R_{mi} \right) = \left(R_A - R_M \right) \qquad \text{(equation 12)}$$

L is determined in an iteration loop of subroutine Robin summarized in Appendix IV.

The second experimental problem is the effect of room temperature variations on the spectrometer system. A deviation of ±1 degree Centigrade in the laboratory temperature changes the gain of the preamplifier enough to shift the position of photopeaks relative to the library spectra of potassium, uranium and thorium. The computer technique which determines the concentrations of potassium, uranium, and thorium demands a constant gain with fixed channel positions of the photopeaks. If the gain changes, then one might be using, for example, a_{30}, b_{30}, and c_{30} with d_{40} to determine the unknown masses in equation 1, M_K, M_U, and M_{Th}. To compensate for the gain drift of the preamplifier and analog to digital converter with room temperature, the data are always normalized to the same gain (6.55 kev/channel) with zero energy in channel 1 of the analog to digital converter. This means that regardless of the room temperature when a sample is run, the same peaks always fall in the same channel location. Since the room temperature changes relatively slowly, there is normally very little drift or gain change during a single run, typically 20,000 seconds. However, over a period of weeks the gain can change significantly if the room temperature steadily increases or decreases. If the room temperature changes

more than 0.5°C during a sample run, the data is worthless because the width and height of the photopeaks are smeared and therefore the sample spectrum cannot be compared with the library spectrum. All samples are measured on at least four separate occasions and those observed to be smeared are discarded.

Depending on the rate of change of the room temperature, the counting time used for a sample can be critical. Results from samples counted for 80,000 seconds or more were invariably bad because of gain changes and drift due to a change in room temperature during the run. Table 6 shows the results for a sample counted for various time intervals. The room temperature increased about 1 degree Centigrade during the experiment, 80,000 seconds. For counting times of 4,000 to 40,000 seconds the calculated heat production varies very little (Table 5). In practice, counting times of 10,000 to 20,000 seconds are used because this time span fit the work and class schedules of the laboratory operators and allows at least four samples to be run each day.

Table 7 shows how the concentrations of potassium, uranium, and thorium and the resultant heat production vary with gain change from the normalized gain of 6.55 kev/channel. The gain is normalized by placing the first prominent peak in channel 93 and the second highest peak in channel 265. The first peak is very sharp and can be identified to within ±1 channel. The second peak is quite broad and visual

Table 6. Variation in measured concentration of K, U, and Th with counting time.

Time (seconds)	F-value	K (%)	U (ppm)	Th (ppm)	Heat Production (HGU)
400	585	6.58	1.71	6.52	3.66
800	1,732	5.64	2.83	7.12	4.24
1,000	2,529	5.69	3.31	7.26	4.56
4,000	8,592	5.59	2.64	7.24	4.13
8,000	14,570	5.80	2.43	6.63	3.94
10,000	16.936	5.70	2.51	6.63	3.97
20,000	23,524	6.35	2.49	5.11	3.85
40,000	30,063	6.27	2.41	6.41	4.00
80,000	3,377	11.14	-0.26	3.62	3.00

Table 7. Variation in measured concentration of K, U, Th due to error in instrument gain.

Gain Change (%)	F-value	Potassium (%)	Uranium (ppm)	Thorium (ppm)	Th/U	Heat Production (HGU)
+9.30	675	7.44	-1.96	6.33	-3.23	1.56
+8.14	557	7.66	-2.46	6.03	-2.45	1.25
+6.98	874	7.17	-1.14	6.43	-5.64	2.02
+5.81	2,230	6.62	0.45	6.81	15.1	2.94
+4.65	1,591	6.73	0.09	6.64	73.8	2.72
+3.49	3,479	6.45	1.01	6.77	6.70	3.24
+2.33	5,825	6.35	1.41	6.76	4.79	3.46
+1.16	22,010	6.37	2.19	6.56	3.00	3.91
0.00*	22,671	6.37	2.22	6.50	2.93	3.92
-1.16	13,718	6.46	2.40	6.31	2.63	4.02
-2.33	3,022	7.08	2.44	5.70	2.34	4.08
-3.49	4,426	6.85	2.48	5.86	2.36	4.08
-4.65	2,088	7.42	2.31	5.35	2.32	4.02
-5.81	1,042	8.54	1.73	4.46	2.58	3.77
-6.98	882	9.02	1.44	4.08	2.83	3.63
-8.14	886	9.06	1.37	4.06	2.96	3.59
-9.30	785	9.57	1.01	3.67	3.63	3.43

*normalized gain=6.55 KeV/channel

inspection of the data can place it to within ±5 channels. In the computer analysis the gain is varied in 0.58% increments (one channel increments) on either side of channel 265 until the F-value, the ratio of two independent chi-square variables, each divided by its degrees of freedom (Hays and Winkler, 1971), reaches a maximum. In this application there are 3 degrees of freedom associated with the regression equation, that is M_K, M_U, and M_{Th} in equation 1. These three degrees of freedom are associated with the first chi-square variable, the sum of the squares attributable to regression. The second chi-square variable is the sum of the squares due to deviation from regression and the degrees of freedom is 507.

$$F = \frac{\left[\frac{(\text{sum of squares attributable to regression})}{3}\right]}{\left[\frac{(\text{sum of squares due to deviation of regression})}{507}\right]}$$

When the F-value reaches a maximum, the regression equation is the best fit of the observed data. The error of +2.33% (four channels) in the gain can cause an error of 36% in uranium, 4% in thorium and 1% in potassium concentration. The resultant error in heat production is about 12%. An error of -2.33% (four channels) in the gain can cause an 11% error in potassium, 10% error in uranium and a 12% error in thorium concentration. The resultant error in heat production is 4%. The resultant error in heat production is always lower than the maximum error in

the concentrations of potassium, uranium and thorium because the errors in concentration partially counter balance each other. For example, a positive gain change increases the calculated concentrations of potassium and thorium and decreases the calculated concentration of uranium. A negative gain change increases the calculated concentration of potassium and uranium and decreases the concentration of thorium.

Background Radiation

The sample container and crystal detector are shielded from external radiation by a lead cylinder three inches thick. The measured background changed very little during the time that the measurements were being made. The measured background spectrum was subtracted from each measured rock spectrum and from the potassium, uranium and thorium standard spectra before any concentration calculations were made (figure 23).

Calculation of Heat Generation

The heat generation for a particular borehole was calculated using the mean measured concentrations of potassium, uranium and thorium. The heat generation of naturally occurring potassium, uranium and thorium is given by MacDonald (1959) as 3.5×10^{-5}, 0.97 and 0.26 erg/gm sec. respectively. A rock density of 2.67 gm/cm^3 was used to convert the heat generation from cal/gm-sec to cal/cm^3-sec (Swanberg, 1973). The density of several

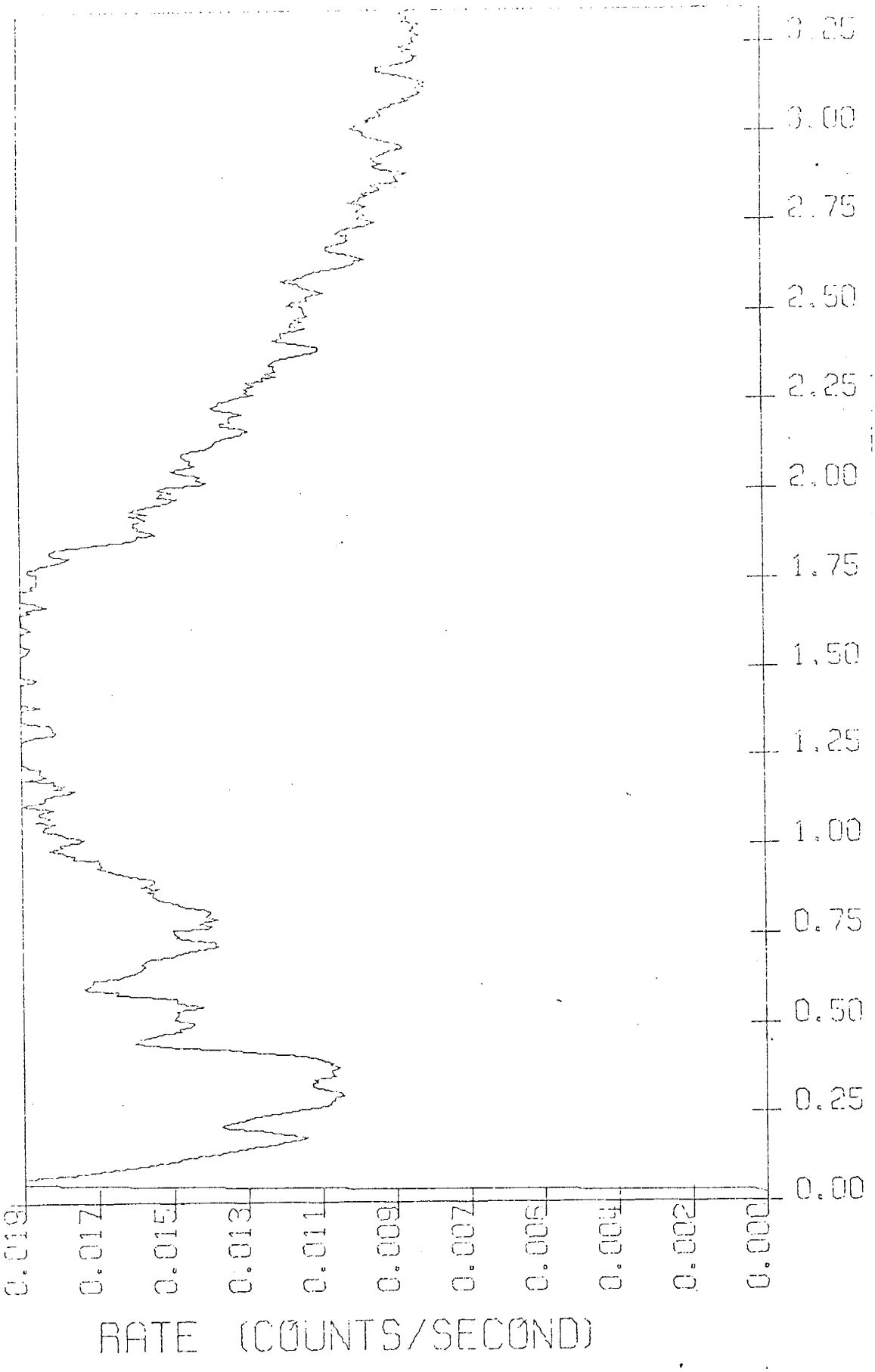

Figure 23 Gamma Ray Spectrum of Background

core samples were measured and they differed by less than 2% from 2.67 gm/cm^3. Tables 8 and 9 list radioactivity data for all samples measured.

Sample Collection and Preparation

Except for the three composite samples, the samples used were rock cores taken from mineral exploration boreholes that penetrated intrusives. The composite samples were from outcrops. The samples were crushed in a standard jaw crusher and then reduced to 100 mesh powder in a Bico-Braun pulverizer. The powder was packed into the sample containers which held 230 cc (approximately 500 grams). The sample containers are all identical thus assuring the same geometry during counting.

Equipment

The gamma ray spectra were measured with a Nuclear Data 512 analyzer system using a 7.5 x 7.5 cm thallium activated sodium iodide crystal. The crystal is mounted in a 7.5 cm thick lead cylinder to isolate the crystal from background radiation while the sample is being counted. When a run has terminated the results are printed on a teletype. The information is then keypunched and processed on the IBM 360-44 computer.

Table 8. Radioactivity Data for Calibration Standards

Sample	Run #	Potassium (g)	Uranium (mg)	Thorium (mg)
Rock Standard #1	1	7.522	0.000530	0.002591
	2	7.316	0.000802	0.002417
	3	4.891	0.000540	0.001714
	4	8.816	0.000333	0.001798
	5	5.124	0.000507	0.001586
	6	6.774	0.000558	0.001994
	7	6.311	0.000563	0.002081
	Mean:	6.679	0.000548	0.002026
Rock Standard #2	1	43.779	0.003155	0.007347
	2	39.256	0.003028	0.006375
	3	40.710	0.002971	0.006201
	4	41.170	0.002793	0.006450
	5	46.509	0.003184	0.007285
	6	45.845	0.003232	0.006998
	7	50.706	0.003458	0.007439
	Mean:	43,996	0.003117	0.006871
Rock Standard #3	1	19.249	0.001321	0.003414
	2	17.883	0.001343	0.003422
	3	17.521	0.001372	0.003330
	4	17.166	0.001256	0.003328
	5	20.085	0.001034	0.003245
	6	18.883	0.000960	0.003100
	7	19.249	0.001265	0.003408
	8	19.694	0.001260	0.003473
	Mean:	18.716	0.001226	0.003340
Rock Standard #4	1	54.352	0.005023	0.010160
	2	48.747	0.004698	0.009413
	3	52.310	0.005115	0.010162
	4	52.495	0.005057	0.010124
	5	51.198	0.005135	0.010309
	6	53.724	0.005023	0.010449
	Mean:	52.138	0.005009	0.010103

Table 8. Radioactivity Data for Calibration Standards (cont.)

Sample	Run #	Potassium (g)	Uranium (mg)	Thorium (mg)
Rock Standard #5	1	6.817	0.000783	0.003789
	2	7.080	0.000661	0.003710
	3	5.818	0.000617	0.003574
	4	6.661	0.000697	0.003685
	5	6.165	0.000731	0.003703
	6	6.750	0.000697	0.003653
	7	6.840	0.000760	0.003776
	Mean:	6.590	0.000707	0.003699

Table 9. Radioactivity Data for Reduced Heat Flow Sites

Site	Sample #	Run #	Potassium (%)	Uranium (ppm)	Thorium (ppm)	Heat Production (HGU)
Crested Butte	70-230m	1	4.42	1.84	6.38	
		2	4.77	1.61	6.41	
	264-380m	1	4.10	2.40	6.04	
		2	3.92	2.20	6.09	
		3	4.13	1.97	5.37	
		4	3.94	2.29	6.51	
		5	4.73	2.08	6.20	
	400-500m	1	4.75	1.49	5.07	
		2	4.16	2.24	5.64	
		3	4.41	2.28	6.72	
		4	4.53	2.46	6.13	
		5	4.16	1.95	5.64	
		6	4.20	2.35	6.26	
	520-620m	1	3.75	1.97	4.34	
		2	3.73	2.15	5.87	
		3	3.73	2.34	4.75	
	640-780m	1	3.06	1.83	3.65	
		2	3.05	1.74	3.86	
		3	3.85	1.33	4.14	
		4	4.65	1.23	4.49	
		Mean:	4.10	1.95	5.41	3.05
Questa #2	#2-1	1	4.04	1.17	22.94	
		2	4.66	0.34	22.75	
		3	4.30	0.02	20.95	
		4	4.81	0.58	24.00	
	#2-2	1	0.0	16.63	33.46	
		2	0.0	17.56	33.44	
		3	0.06	13.68	29.08	
		4	0.0	15.18	27.56	
		5	0.0	16.25	31.03	
	#2-3	1	0.57	9.43	33.51	
		2	0.68	11.18	38.49	
		3	1.77	10.06	33.87	
		4	2.29	9.69	31.86	
		5	2.44	10.54	30.76	
		Mean:	0.78	13.02	32.31	12.97

Table 9. Radioactivity Data for Reduced Heat Flow Sites (cont.)

Site	Sample #	Run #	Potassium (%)	Uranium (ppm)	Thorium (ppm)	Heat Production (HGU)
Questa #1	168-169m	1	1.65	11.16	30.33	
		2	1.29	11.46	31.20	
		3	1.11	10.34	26.03	
		4	1.49	10.37	25.82	
	329-331m	1	2.00	15.86	25.04	
		2	1.79	15.52	27.38	
		3	2.39	16.80	24.30	
	250-252m	1	5.67	10.34	22.13	
		2	1.65	13.52	23.03	
		3	1.21	13.48	23.43	
	454-456m	1	1.07	13.83	23.44	
		2	0.94	14.55	24.33	
		3	0.79	14.20	21.28	
		4	1.48	13.89	24.90	
		Mean:	1.49	13.61	25.07	12.85
Los Alamos	746-744m	1	4.95	0.0	22.30	
		2	3.91	0.52	15.45	
		3	3.10	0.77	22.72	
		4	3.63	0.31	20.74	
		5	3.19	0.32	19.25	
		6	3.53	0.70	16.52	
	765-766m	1	3.81	1.56	9.00	
		2	3.23	1.35	7.59	
		3	3.05	1.00	6.23	
		4	3.99	1.82	9.85	
		5	3.95	1.56	9.90	
		6	3.39	1.09	7.91	
	753-750m	1	3.70	0.20	20.29	
		2	0.21	0.14	39.51	
		3	3.06	0.0	20.90	
		4	2.88	0.0	24.95	
		5	3.03	0.18	21.22	
		6	3.14	0.0	36.69	
	757-759m	1	3.65	1.44	14.35	
		2	4.67	1.73	13.76	
		3	3.25	1.54	17.11	
		Mean:	3.52	0.92	15.95	4.06

Table 9. Radioactivity Data for Reduced Heat Flow Sites (cont.)

Site	Sample #	Run #	Potassium (%)	Uranium (ppm)	Thorium (ppm)	Heat Production (HGU)
San Pedro #3	113-153m	1	2.17	3.51	11.28	
		2	2.26	3.82	10.85	
		3	2.20	3.42	11.09	
		4	2.00	3.77	9.74	
	173-194m	1	1.90	2.79	8.58	
		2	2.07	2.80	8.91	
		3	2.48	2.34	8.21	
		4	1.96	28.4	8.90	
	252-299m	1	2.00	2.21	10.66	
		2	2.84	1.39	7.94	
	311-366m	1	2.51	2.21	11.39	
		2	2.75	1.37	9.50	
		3	2.56	2.52	12.73	
		4	3.70	1.09	11.03	
	376-406m	1	2.44	2.15	12.64	
		2	2.92	2.30	12.31	
		3	2.28	3.00	13.62	
		4	3.12	2.43	12.11	
	450-491m	1	3.10	1.75	12.07	
		2	2.82	2.60	12.84	
		3	3.19	3.21	13.11	
		4	3.17	3.03	14.56	
		Mean:	2.55	2.51	10.95	3.98
San Pedro #4	#4-1	1	3.54	3.27	12.69	
		2	3.63	3.48	13.18	
		3	3.46	3.58	13.37	
		4	3.43	3.63	11.27	
	#4-2	1	3.38	3.35	12.05	
		2	3.95	2.95	10.95	
		3	3.06	3.75	12.18	
	#4-3	1	3.19	3.06	12.59	
		2	3.13	3.89	11.31	
	#4-4	1	3.38	2.93	10.80	
		2	3.17	3.39	12.26	
		3	3.04	3.19	12.32	
		4	3.25	3.29	12.71	
		5	3.12	3.42	10.75	
		Mean:	3.33	3.39	12.02	4.88

Table 8. Radioactivity Data for Reduced Heat Flow Sites (cont.)

Site	Sample #	Run #	Potassium (%)	Uranium (ppm)	Thorium (ppm)	Heat Production (HGU)
Sierra Blanca	3-6m	1	3.84	7.27	19.59	
		2	3.04	6.00	16.77	
	6-9m	1	2.77	7.20	36.56	
		2	1.04	8.80	36.59	
	9-12m	1	4.07	7.38	20.33	
		2	5.37	6.91	19.34	
		3	4.35	7.31	19.61	
		4	4.49	6.12	16.84	
	12-15m	1	3.50	16.09	40.82	
		2	0.0	23.25	41.99	
		3	0.0	19.56	40.19	
		4	0.0	19.28	40.27	
		Mean:	3.36	9.97	28.65	11.76
Animas Peak	39-79m	1	3.90	5.96	17.51	
		2	3.33	4.88	15.24	
		3	6.93	5.40	13.85	
		4	4.03	5.53	14.93	
		5	3.39	5.83	13.52	
	39-213m	1	4.59	5.09	15.02	
		2	4.70	6.83	17.08	
	89-144m	1	3.81	4.32	10.95	
		2	3.96	4.52	13.56	
		3	3.86	5.31	13.37	
		4	4.61	4.36	12.89	
		5	3.54	4.51	13.88	
	162-204m	1	4.32	3.73	12.18	
		2	3.86	4.69	14.42	
		3	3.52	4.95	14.59	
		4	3.57	4.68	14.77	
		5	3.42	4.71	11.06	
	213-294m	1	3.67	5.75	16.02	
		2	4.71	4.85	14.49	
		3	3.58	5.61	15.36	
		4	3.88	5.51	15.09	
		Mean:	3.96	5.18	14.50	6.55

Table 9. Radioactivity Data for Reduced Heat Flow Sites (cont.)

Site	Sample #	Run #	Potassium (%)	Uranium (ppm)	Thorium (ppm)	Heat Production (HGU)
Orogrande	264-324m	1	2.47	1.82	6.87	
		2	2.22	1.94	7.50	
		3	3.59	1.57	5.97	
		4	2.39	2.23	7.67	
		5	3.29	2.25	8.46	
	264-366m	1	4.26	0.58	6.69	
		2	3.18	1.86	7.75	
		3	2.97	2.34	8.05	
		4	3.24	1.71	7.05	
		5	3.04	2.29	8.71	
		6	3.23	1.54	6.80	
	312-321m	1	2.53	2.61	7.41	
		2	2.70	3.04	7.97	
		3	3.27	2.72	9.43	
	333-342m	1	4.49	1.51	7.40	
	346-354m	1	3.02	1.90	6.83	
		2	3.56	1.55	6.16	
	359-366m	1	2.47	1.89	7.21	
		2	2.47	1.87	7.92	
		3	2.57	1.68	6.70	
		4	2.77	1.86	7.91	
		5	2.42	1.99	7.21	
		6	2.60	1.60	6.57	
		Mean:	3.18	1.96	7.37	3.18
Composite North		1	3.55	1.04	11.02	
		2	3.75	1.22	11.39	
		3	3.71	1.04	10.56	
		Mean:	3.67	1.10	10.95	3.36
Composite Central		1	4.05	1.47	9.94	
		2	3.01	1.79	11.06	
		3	2.89	1.72	8.75	
		Mean:	3.32	1.66	9.91	3.46
Composite South		1	3.16	1.43	11.77	
		2	2.85	1.94	11.63	
		Mean:	3.01	1.69	11.70	3.70

APPENDIX IV

COMPUTER PROGRAMS

Thermal Conductivity program

The thermal conductivity program (COND) uses the two formulas discussed in Appendix I for the divided bar and the absolute thermal conductivity system along with the formula for the thermal conductivity of fragment samples as reported by Sass and others (1971b). The unknown parameters are measured in the laboratory and keypunched. The program calculates and lists the thermal conductivities and the average thermal conductivity over those zones specified by the user.

Temperature Gradient program

The thermistor program (TRMX) uses the keypunched resistance-depth data taken in the field. The program uses the resistance-temperature calibration curve supplied by the manufacturer of the temperature probe and converts the field data to a temperature depth plot as in figures 10-15 and supplies a least mean squares temperature gradient in those depth zones indicated by the user.

Subroutine LLMSQ

Purpose

Calculate least mean squares temperature gradient

Usage

```
Call LLMSQ(x, y, title, Iend, Istart, grad, kk)
```

Description of parameters

x	temperature in degrees centigrade
y	depth in meters
title	name of temperature log
Iend	bottom of zone of interest
Istart	top of zone of interest
grad	temperature gradient
kk	number of data pairs

Remarks

Do not submit duplicate depths

Subroutines and function subprograms required

None

Subroutine DSRT

Purpose

Sort temperature versus depth data and average multiple readings at a common depth

Usage

```
Call DSRT(d, t, np, n)
```

Description of parameters

d	depth array
t	temperature array
np	number of measurements made
n	number of discrete depths

Remarks

Input d and t array destroyed in computation

Subroutines and function subprograms required

None

Radioactivity program

The radioactivity program (RADI) inputs the background spectra, the potassium spectra, the uranium spectra, the thorium spectra, and the unknown rock spectra and calculates the potassium, uranium, and thorium concentrations of the rock sample as described in Appendix II. The program that performs the linear regression analysis was written by Dr. Alan Gutjahr and adapted by myself to make the radioactivity calculations. The subprograms MINV, CORRE, ORDER, and MULTR are subroutines available on line in the New Mexico Tech computer center by accessing the IBM scientific subroutine package. The following listing summarizes the subprograms used.

Subroutine data

Purpose

Read data from an input device and process for subroutine corre.

Usage

Call data(m, d)

Description of parameters

m	number of variables
d	array containing the variables

Remarks

None

Subroutines and function subprograms required

gain(y, np, p1, p2, p3, p4)

smooth(y, np)

rate(y, np)

back(y, np, bk)

Subroutine rate

Purpose

Calculate the true counting rate given the measured number of counts and the live time.

Usage

Call rate(y, np)

Description of parameters

y	input array of the number of counts in each channel
np	number of data points

Remarks

Counting time must be passed in a common block

Subroutines and function subprograms required

Robin(y, sum, tau, alpha, np)

Subroutine gain

Purpose

Normalize the gain of the output spectra of the spectrometer to 6.55 kev per channel with zero energy in channel zero

Usage

Call gain(y, np, p1, p2, p3, p4)

Description of parameters

y	input matrix of data
np	number of data points
p1	channel number of first peak
p2	channel number of second peak
p3	channel number of third peak

p4 channel number of fourth peak

Remarks

None

Subroutines and function subprograms required

None

Subroutine smooth

Purpose

To compute a vector of smoothed function values given a vector of function values whose entries correspond to equidistantly spaced argument values

Usage

Call smooth(y, np)

Description of parameters

y input vector of data to be smoothed. This vector is destroyed in computation and is replaced by the resultant smoothed values

np number of data points

Remarks

None

Subroutines and function subprograms required

None

Subroutine back

Purpose

Remove the background noise from the measured spectrum

Usage

Call back(y, np, bk)

Description of parameters

y input data array

np number of data points

bk background data array

Remarks

None

Subroutines and function subprograms required

None

Subroutine graf

Purpose

Plot the data on the calcomp plotter

Usage

Call graf(xhi, xlow, yhi, ylow, np, x, y, nplt, title)

Description of parameters

xhi maximum value of x

xlow minimum value of x

yhi maximum value of y

ylow minimum value of y

np number of data points

x independent variable array

y dependent variable array

nplt symbol code for plotter

title title of data set

Remarks

None

Subroutines and function subprograms required

None

Subroutine conc

Purpose

Calculate the concentrations of potassium, uranium, and thorium

Usage

Call conc(d, sb)

Description of parameters

d	input array of regression coefficients
sb	input matrix of standard deviations of the regression coefficients

Remarks

Sample weight must be passed in a common block
Resultant concentrations are printed out.

Subroutines and function subprograms required

None

Subroutine minv

Purpose

Invert a matrix

Usage

call minv(a, n, d, l, m)

Description of parameters

a	input matrix, destroyed in computation and replaced by resultant inverse
n	order of matrix a
d	resultant determinant
l	work vector of length n
m	work vector of length n

Remarks

matrix a must be a general matrix

Subroutines and function subprograms required

None

Subroutine CORRE

Purpose

Compute means, standard deviations, sums of cross-products of deviations, and correlation coefficients

Usage

```
Call CORRE(n, m, io, x, xbar, std, rx, r, b, d, t)
```

Description of parameters

n	number of observations
m	number of variables
io	option code for input data o if data are to be read in from an input device in the special subroutine data i if all data are already in core
x	if io=0, the value of x is 0.0 if io=1, x is the input matrix (n by m) containing data
xbar	output vector of length m containing means
std	output vector of length m containing standard deviations
rx	output matrix (m by m) containing sums of cross-products of deviations from means
r	output matrix (only upper triangular portion of the symmetric matrix of m by m) containing correlation coefficients (storage mode of 1)
b	output vector of length m containing the diagonal of the matrix of sums of cross-products of deviations from means
d	working vector of length m
t	working vector of length m

Remarks

None

Subroutines and function subprograms required

Data(m, d)

Subroutine ORDER

Purpose

Construct from a larger matrix of correlation coefficients a subset matrix of intercorrelations among independent variables and a vector of intercorrelations of independent variables with dependent variable. This subroutine is normally used in the performance of multiple and ploynomial regression analyses.

Usage

Call ORDER (m, r, ndep, k, isave, rx, ry)

Description of parameters

m	number of variables and order of matrix r
r	input matrix containing correlation coefficients This subroutine expects only upper triangular portion of the symmetric matrix to be stored (by column) in r (storage mode of 1).
ndep	the subscript number of the dependent variable
k	number of independent variables to be included in the forthcoming regression
isave	input vector of length K+1 containing, in ascending order, the subscript numbers of k independent variables to be included in the forthcoming regression. Upon returning to the calling routine this vector contains, in addition, the subscript number of the dependent variable in K+1 position
rx	output matrix (k x k) containing inter-correlations among independent variables to be used in forthcoming regression

ry — output vector of length k containing intercorrelations of independent variables with dependent variables

Remarks

None

Subroutines and function subprograms required

None

Subroutine MULTR

Purpose

Perform a multiple linear regression analysis for a dependent variable and a set of independent variables This subroutine is normally used in the performance of multiple and polynomial regression analyses.

Usage

```
Call MULTR(n, k, xbar, std, d, rx, ry, isave, b,
sb, t, ans)
```

Description of parameters

n — number of observations

k — number of independent variables in this regression

xbar — input vector of length m containing means of all variables. m is number of variables in observations.

std — input vector of length m containing standard deviations of all variables

d — input vector of length m containing the diagonal of the matrix of sums of cross-products of deviations from means for all variables

rx — input matrix (k x k) containing the inverse of intercorrelations among independent variables

ry — input of length k containing intercorrelations of independent variables with dependent variable

isave — input vector of length k+1 containing subscripts of independent variables in ascending order. The subscript of the dependent variable is stored in the last, k+1, position.

b — output vector of length k containing regression coefficients

sb — output vector of length k containing standard deviations of regression coefficients

t — output vector of length k containing t-values

ans — output vector of length 10 containing the following information.

- ans(1) intercept.
- ans(2) multiple correlation coefficient.
- ans(3) standard error of estimate.
- ans(4) sum of squares attributable to regression (SSAR).
- ans(5) degrees of freedom associated with SSAR.
- ans(6) mean square of SSAR.
- ans(7) sum of squares of deviations from regression (SSDR).
- ans(8) degrees of freedom associated with SSDR.
- ans(9) mean square of SSDR.
- ans(10) f-value.

Remarks

n must be greater than k + 1

Subroutines and function subprograms required

None.

Subroutine ROBIN

Purpose

Calculate the real distribution function of the data given the measured distribution function.

Usage

```
Call ROBIN(y, sum, tau, alpha, np)
```

Description of parameters

y	data input array.
sum	summation of y(i), i=1,np.
tau	exponent used to correct measured counting rate r(actual)=r(measured)**tau.
alpha	factor in the distribution function, y(i) = y(i)/(u.o-y(i)*alpha).
np	number of data points

Remarks

Tau is defined in subroutine RATE

. Subroutines and function subprograms required

GRAF(xhi, xlow, yhi, ylow, np, x, y, nplt, title).

REFERENCES CITED

Aoki, K., 1967, Petrography and petrochemistry of latest Pliocene olivine-tholeiites of Taos area, northern New Mexico, U.S.A.: Contr. Mineral. and Petrol., v. 14, p. 190-203.

Archambeau, C. B., Flinn, E. A., and Lambert, P. G., 1969, Fine structure of the upper mantle: Jour. Geophys. Research, v. 74, p. 5835-5866.

Birch, F., 1947, Temperature and heat flow in a well near Colorado Springs: Am. Jour. Sci., v. 245, p. 1-18.

_____, 1950, Flow of heat in the Front Range, Colorado: Geol. Soc. America Bull., v. 61, p. 567-630.

Birch, F., Roy, R. F., and Decker, E. R., 1968, Heat flow and thermal history in New York and New England, in Studies of Appalachian Geology: Northern and Maritime, edited by E. Zen, W. S. White, J. B. Hadley and J. B. Thompson, Jr., p. 437-451: Interscience, New York, 475 p.

Bredehoeft, J. D., and Papadopulos, I. S., 1965, Rates of vertical groundwater movement estimated from the earth's thermal profile: Water Resources Research, v. 1, p. 325-328.

Caner, B., Cannon, W. H., Livingstone, C. E., 1967, Geomagnetic depth sounding and upper mantle structure in the Cordillera Region of Western North America: Journ. Geophys. Research, v. 72, no. 24, p. 6335-6340.

Chapin, C. E., 1971, The Rio Grande Rift, Part I: Modifications and Additions: New Mexico Geological Society - Twenty-second Field Conference, p. 191-201.

Christiansen, R. L., and Lipman, P. W., 1972, Cenozoic volcanism and plate-tectonic evolution of the Western United States. II. Late Cenozoic: Phil. Trans. R. Soc. Lond., v. 271, p. 249-284.

Decker, E. R., 1969, Heat flow in Colorado and New Mexico: Jour. Geophys. Research, v. 75, p. 550-559.

Decker, E. R., and Smithson, S. B., 1975, Heat flow and gravity interpretation across the Rio Grande Rift in southern New Mexico and West Texas: Jour. Geophys. Research, vol. 80, no. 17, p. 2542-2552.

Eardley, A. J., 1962, Structural Geology of North America: New York, Harper and Row, p. 553-582.

Hays, L. H., Winkler, R. L., 1971, Statistics, probability, inference, and decision: New York, Holt, Rinehart, and Winston, Inc.

Healy, J. H., and Warren, D. H., 1969, Explosion studies in North America: In the Earth's Crust and Upper Mantle, Geophys. Mono. Series No. 13, Am. Geophys. Union, p. 208-219.

Herrin, E., and Clark, S. P., 1956, Heat flow in West Texas and Eastern New Mexico: Geophysics, v. 21, p. 1087-1099.

Herrin, E. T., Taggart, J., 1962, Regional variations in Pn velocity and their effect on the location of

epicenters: Bull. Seis. Soc. America, v. 52, p. 1037-1046.

Herrin, E., 1969, Regional variations of P-wave velocity in the upper mantle beneath North America: in The Earth's Crust and Upper Mantle, Geophys. Mono. Series No. 13, Am. Geophys. Union, p. 242-246.

Jackson, W. H., Stewart, S. W., and Pakiser, L. C., 1963, Crustal structure in eastern Colorado from Seismic-refraction measurements: Jour. Geophys. Research, v. 68, p. 5767-5776.

James, D. E., Steinhart, J. S., 1967, Structure beneath the continents: A critical review of explosion studies 1960-1965: in The earth beneath the continents edited by Steinhart and Smith, Geophys. Monogr. 10, Am. Geophys. Union, p. 293-333.

Jeffreys, H., The Earth, 1952: Cambridge, The University Press.

Johnson, R. B., Dixon, G. H., Wanek, A. A., 1966, Late Cretaceous and Tertiary stratigraphy of the Raton Basin of New Mexico and Colorado: New Mexico Geological Society - Seventh Field Conference, p. 88.

Johnson, R. B., 1968, Geology of the igneous rocks of the Spanish Peaks region Colorado: Geological Survey Professional Paper 594-G, Washington, United States Printing Office.

Kelley, V. C., 1952, Tectonics of the Rio Grande depression of central New Mexico: New Mexico Geol. Soc. Guidebook

of the Rio Grande Country, 3rd Field Conf., p. 93-105.

_____, 1972, New Mexico lineament of the Colorado Rockies front: Geol. Soc. America Bull., v. 83, p. 1849-1852.

Lachenbruch, A. H., 1968, Preliminary geothermal model of the Sierra Nevada: Jour. Geophys. Research, v. 73, p. 6977-6989.

_____, 1970, Crustal temperature and heat production: Implications of the linear heat flow relation: Jour. Geophys. Research, v. 75, p. 3291-3300.

Luedke, R. G., and Burbank, W. S., 1968, Volcanism and cauldron development in the western San Juan Mountains, Colorado: Quarterly of the Colorado School of Mines, v. 63, p. 175-207.

Lipman, P. W., 1969, Alkalic and tholeiitic basaltic volcanism related to the Rio Grande Depression: Southern Colorado and Northern New Mexico, Geol. Soc. America Bull., v. 80, p. 1343-1353.

Lipman, P. W., Bunker, C. M., and Bush, C. A., 1973, Potassium, thorium, and uranium contents of upper Cenozoic basalts of the Southern Rocky Mountain region, and their relation to the Rio Grande depression: Jour. Research U. S. Geol. Survey vol. 1, no. 4, July-Aug. 1973, p. 387-401.

MacDonald, G. J. F., 1959, Calculations on the thermal history of the Earth: Jour. Geophys. Research, v. 64, p. 1967.

Pakiser, L., 1963, Structure of the crust and upper mantle in the Western United States: Jour. Geophys. Research, v. 68, p. 5747-5756.

Parzen, E., 1962, Stochastic Processes: San Francisco, Holden-Day, Inc., 324 p.

Phinney, R. A., 1964, Structure of the Earth's crust from spectral behavior of long-period body waves: Jour. Geophys. Research, v. 69, p. 2997-3017.

Ratcliffe, E. H., 1959, Thermal conductivity of fused and crystalline quartz: British Jour. of Applied Physics, v. 10, p. 22-25.

Reiter, M., Hartman, H., 1971, A new steady state method for determining thermal conductivity: Jour. Geophys. Research, v. 76, no. 29, p. 7047-7051.

Reiter, M., Edwards, C. L., Hartman, H., Weidman, C., 1975, Terrestrial heat flow along the Rio Grande Rift, New Mexico and Southern Colorado: Geol. Society of America Bull., v. 86, p. 811-818.

Roy, R. F., Decker, E. R., Blackwell, D. D., and Birch, F., 1968, Heat flow in the United States: Jour. Geophys. Research, v. 73, p. 5207-5221.

Roy, R. F., Blackwell, D. D., and Decker, E. R., 1972, Continental heat flow: in The Nature of the Solid Earth, McGraw Hill, New York, p. 506-544.

Rybach, L., 1971, Radiometric techniques: in Modern methods of geochemical analysis, New York-London, edited by Wainerdi and Uken.

Sanford, A. R., and Holmes, C. R., 1962, Micro-earthquakes near Socorro, New Mexico: Jour. Geophys. Research, v. 67, p. 4449-4459.

Sanford, A. R., 1963, Seismic activity near Socorro: New Mexico Geological Society - Fourteenth Field Conference, p. 146-151.

_____, 1965, An instrumental study of New Mexico earthquakes: New Mexico State Bureau of Mines and Mineral Resources, Circular 78, 12 p.

_____, 1968, Gravity survey in central Socorro County, New Mexico: New Mexico State Bureau of Mines and Mineral Resources, Circular 91, 14 p.

Sanford, A. R., and Cash, D. J., 1969, An instrumental study of New Mexico earthquakes July 1, 1964 through Dec. 31, 1961: New Mexico State Bureau of Mines and Mineral Resources, Circular 102, 7 p.

Sanford, A. R., Alptekin, O., and Toppozada, T. R., 1973, Use of reflection phases on micro-earthquake seismograms to map an unusual discontinuity beneath the Rio Grande Rift: Bull. Seis. Soc. America, v. 63, p. 2021-2034.

Sass, J. H., Lachenbruch, A. H., Monroe, R. J., Greene, G. W., and Moses, T. H., 1971a, Heat flow in the Western United States: Jour. Geophys. Research, v. 76, p. 6376-6413.

_____, 1971b, Thermal conductivity of rocks from measurements on fragments and its application to heat flow

determinations: Jour. Geophys. Research, v. 76, p. 3391-3401.

Schmucker, U., 1964, Anomalies of geomagnetic variations in the Southwestern United States: Journal Geomagn. Geoelec., v. 15, p. 193-221.

_____, 1970, Anomalies of geomagnetic variations in the Southwestern United States: Bull. Scripps Inst. Oceanogr., v. 13, p. 1-165.

Sidwell, R., and Warn, G. F., 1953, Pennsylvanian and related sediments of Upper Pecos Valley, New Mexico: Am. Assoc. Petroleum Geol. Bull., v. 37, n. 5, p. 975-1013.

Smithson, S. B., and Decker, E. R., 1972, Heat flow and gravity studies across the Rio Grande Rift in Southern New Mexico and Western Texas: EOS (Am. Geophys. Union Trans.), v. 53, p. 516.

Stacey, F. D., 1969, Physics of the Earth: New York, John Wiley and Sons, Inc., 1324 p.

Steven, T. A., and Epis, R. C., 1968, Oligocene volcanism in South-central Colorado: Quarterly of the Colorado School of Mines, v. 63, p. 241-255.

Stewart, S. W., Pakiser, L. C., 1962, Crustal structure in eastern New Mexico interpreted from the Gnome explosion, Bull. Seis. Soc. America, v. 52, p. 1017-1030.

Stuart, D. J., Roller, J. C., Jackson, W. H., and Mangan, G. B., 1964, Seismic propagation paths, regional

traveltimes, and crustal structure in the Western United States: Geophysics, vol. xxix, no. 2, p. 178-187.

Stormer, J. C., 1972, Ages and nature of volcanic activity on the Southern High Plains, New Mexico and Colorado: Geol. Soc. America Bull., v. 83, p. 2443-2448.

Swanberg, C. A., 1972, Vertical distribution of heat generation in the Idaho batholith: Jour. Geophys. Research, v. 77, p. 2508-2513.

Toppozada, T. R., and Sanford, A. R., 1972, Instrumental study of New Mexico earthquakes January 1968 through June 1971: New Mexico State Bureau of Mines and Mineral Resources, Circular 126, 6 p.

Walsh, J. B., Decker, E. R., 1966, Effect of pressure and saturating fluid on the thermal conductivity of compact rock: Jour. Geophys. Research, v. 71, p. 3043-3062.

Warren, A. E., Sclater, J. C., Vacquier, V., and Roy, R., 1969, A comparison of terrestrial heat flow and transient geomagnetic fluctuations in the Southwestern United States, Geophysics, v. 34, p. 463-478.

ERRATA SHEET

REFERENCES CITED

page 92 -

Birch, F., 1950, Flow of heat in the Front Range, Colorado: Geol. Soc. America Bull., v. 61, p. 567-630.

page 93 -

Costain, J. K., and Wright, P. M., 1973, Heat flow at Spor Mountain, Jordan Valley, Bingham, and LaSal, Utah: Jour. Geophys. Research, v. 78, p. 8687-8698.

page 95 -

Lovering, P. S., 1948, Geothermal gradients, recent climatic changes, and rate of sulfide oxidation in the San Manuel District, Arizona: Econ. Geol., v. 43, p. 1-20.

page 98 -

Spicer, H. C., 1964, Geothermal gradients and heat flow in the Salt Valley anticline, Utah: Boll. Geofisica, Peorica, ed. Applicata, v. 6, p. 263-282.

This dissertation is accepted on behalf of the faculty of the Institute by the following committee:

Adviser

August 28, 1975
Date